EFFECT OF TITANIUM, ZIRCONIUM AND NIOBIUM ON LATTICE PARAMETER, DENSITY AND MAGNETIC SATURATION MOMENT OF $Ni_{0.5}$ $Zn_{0.5}$ Fe_2 O_4

By

PROBAL KUMAR DAS

DEPARTMENT OF METALLURGICAL ENGINEERING

INDIAN INSTITUTE OF TECHNOLOGY KANPUR

JANUARY, 1981

EFFECT OF TITANIUM, ZIRCONIUM AND NIOBIUM ON LATTICE PARAMETER, DENSITY AND MAGNETIC SATURATION MOMENT OF $Ni_{0.5}$ $Zn_{0.5}$ Fe_2 O_4

A Thesis Submitted
in Partial Fulfilment of the Requirements
for the Degree of
MASTER OF TECHNOLOGY

By
PROBAL KUMAR DAS

to the

DEPARTMENT OF METALLURGICAL ENGINEERING
INDIAN INSTITUTE OF TECHNOLOGY KANPUR
JANUARY, 1981

ME-1981- M-DAS·ERF

CERTIFICATE

Certified that the thesis entitled "Effect of Titanium, Zirconium and Niobium on Lattice Parameter, Density and Magnetic Saturation Moment of $Ni_{0.5}Zn_{0.5}Fe_2O_4$" has been carried out under my supervision and it has not been submitted elsewhere for a degree.

(A. R. Das)
Professor
Department of Metallurgical Engineering
Indian Institute of Technology
KANPUR.

ACKNOWLEDGEMENTS

I express my hearty gratitude to Dr. A.R. Das for suggesting such an interesting topic and for constant guidance throughout the course of this work.

I owe to Dr. K.P. Gupta for his wise comments and extensive helps and to Dr. D.C. Khan for allowing me to use the magnetometer.

I thank Mr. R.K. Prasad and Mr. Malviya of Ceramic Lab., Mr. Chaurasia and Mr. A.C. Basak of Analytical Chemistry (Met. Engg.) lab., Mr. Mongle of Thermodynamics Lab., Mr. Pandey of X-ray Lab., Mr. B. Sharma, Mr. Warthwal, Mr. I. Ahmed, Mr. Agnihotri and Mr. Narsingh of A.C.M.S. for their helps.

I also got assistances from my friends Mr. G.C. Das, Mr. Sodhi, Mr. N.C. Biswas, Mr. N.K. Ghosh, Mr. P. Sarkar, Mr. S. Bhattacharya, Mr. V.V. Bhaskar, Mr. Swaminathan, Mr. K.T. Kembian, Mr. A.R. Paladhi and Mr. D. Roy. I am indebted especially to Mr. A. Sen who has guided me intimately.

Finally I thank Mr. R.N. Srivastava and Mr. U.S. Misra for their neat typing.

December, 1980
I.I.T. Kanpur

Probal Kumar Das

CONTENTS

LIST OF TABLES

LIST OF FIGURES

Page

ABSTRACT

Stoichiometric 50:50 Ni-Zn ferrite was prepared following usual ceramic methods. Titanium, Zirconium and Niobium were doped in four percentages each in the base ferrite taking them in sulphuric acid medium. The mixtures were fired once at 800°C for 1 hour to dissociate the raw materials and finally at 1250°C for 4 hours to complete ferritization. The accurate lattice parameters of the samples were determined by point count method using Nelson Riley function. Densities of the samples were determined by pycnometer using vacuum and Toluene as liquid. The magnetic saturation moments were measured in vibrating magnetometer at a maximum field of 6.5 K.Oes. The base ferrite had density 5.2576 gms/ml, lattice parameter 8.3975 Å (Siefert, Germany) and 8.3936 Å (XRD 5, England) and magnetic saturation moment, 71.44 emu/gm.

Titanium doped samples showed a sharp fall in lattice parameter upto 0.0240 mole fraction with monotonic increase afterwards but with decreased solubility (upto 0.4217 mole fraction). The densities followed just the reverse nature.

Zirconium and Niobium were slightly soluble (Zr^{4+} upto 0.0886 mole fraction, Nb^{5+} upto 0.0012 mole fraction) in Ni-Zn ferrite as is reflected from the constancy of the lattice parameter values (at 8.399 Å for Zr and 8.398 Å

for Nb). The densities initially decreased upto 5.1377 gms/ml for Zr at 0.0231 mole fraction and 5.0770 gms/ml. for Nb. For Zirconium, the density then suddenly increased unexpectedly and flattened off. For Niobium the gradual increase in density was explained to be due to its change in valency state.

All the dopants showed same nature of variation in magnetic saturation moment values. Initial sharp drop was followed by slight increase, flattenning and drop off. The initial drop was sharpest for Zirconium followed by Niobium and Titanium. The latter drop was sharpest for Ti upto 47.23 emu/gm at 0.4217 mole fraction. For Zirconium, the value was 53.88 emu/gm at 0.3696 mole fraction and for Niobium, 53.46 emu/gm at 0.0188 mole fraction.

These behaviours were explained by considering the dopant ions going into the B site replacing one Fe^{3+} and one fourth of Ni^{2+} and Zn^{2+} each. At higher percentages, due to immiscibility of the dopant ions, mixture rule was applied and it could explain the changes well. Ti^{4+} ion (0.61 Å) showed highest solubility than Zr^{4+} (0.72 Å) and Nb^{5+} (0.64 Å).

Chapter 1

INTRODUCTION

Ferrites are ceramic magnetic materials. Although they are inferior to those of magnetic metals or alloys in some respect at low frequencies, they are widely used in telecommunication industries due to their considerably high permeabilities at higher frequencies and low electrical conductivity leading to very low losses. Ni-Zn ferrites are among the most common ferrites which are categorised as soft ferrites due to their soft magnetic behaviour. These are designed for very high frequency operations to more than 100 MHz. Initial permeabilities are about 10 to 4000 and coercivities are several oersteds. The Ni-Zn ferrites have very high resistivity of about 10^9 ohm-cm under best conditions.[1]

The ferrites are ferrimagnetic oxides with a spinel structure, the general formula of which is $A^{2+}\ B_2^{3+}\ O_4^{2-}$, where A denotes tetrahedral and B denotes octahedral sites. The structure is of two types, viz., (a) normal and (b) inverse spinel. In both the structures 32 O^{2-} ions form the unit cell where they are arranged in a cubic close packed array forming 64 tetrahedral and 32 octahedral sites. Among these only 16 octahedral and 8 tetrahedral holes are filled up by cations. In case of normal spinels the divalent cations

occupy the tetrahedral sites (A) and trivalent cations, the octahedral sites (B), but in inverse spinels the tetrahedral holes are occupied by the half of the trivalent cations whereas the octahedral holes are occupied by the remaining half of the rest trivalent cations together with the divalent cations. In fact, crystals having inverse spinel structure show magnetic behaviour. This is due to the mutual cancellation of the magnetic moments of trivalent cations at the tetrahedral and octahedral sites which are opposite in direction and the net moment is due to the magnetic moment of the cations in the octahedral site.

As Ni^{2+} and Zn^{2+} have similar physical and chemical properties, they can replace each other. This is verified by the X-ray data. Ni^{2+} has a strong preference for B sites whereas Zn^{2+} almost exclusively selects A position causing several properties to be the function of Zinc content.[2]

The site preferences of these transition metal ions in oxide form can be explained by two theories. Dunitz and Orgel[3] used crystal field theory concept which is based on purely ionic type bonding. Blasse[4] used a simplified molecular orbital approach taking into account the covalent bonding between oxygen and these cations. Both these theories predict tetrahedral site preferences for d^5, d^6, d^7, d^9 and d^{10} ions and octahedral for Cr^{3+} but no agreement is found for Ni^{2+}.

The fact that Zn^{2+} ion has a strong preference of tetrahedral site is taken help of to improve several properties of Ni-ferrite. When Zn^{2+} ion is added to Ni-ferrite it goes to the tetrahedral sites replacing Fe^{3+} ion which occupies the octahedral site. Thus as more and more Zn^{2+} is added to the Ni-ferrite more will be the imbalance between the amounts of Fe^{3+} in tetrahedral and in octahedral sites and the magnetic moment of the structure will increase accordingly, [Figure 1(a)]. However, the addition of more than 50 mole % Zinc in Ni-ferrite reduces the net magnetic moment from the peak value as the AB interaction is overcome by BB anti-parallel interaction[5]. So from magnetic saturation point of view this composition is very important.

One of the most important properties of ferrites is magnetic anisotropy which strongly control the magnetic properties of these materials. The anisotropy constant varies from one material to another and hence with the chemical composition of the material. It is also dependent upon temperature. Two important factors regarding this are crystal structure and type of magnetic materials.

Another factor which plays an important role is the partial pressure of oxygen at the time of sintering and cooling. The oxygen partial pressure affects the magnetic properties in two ways, (a) in reducing condition and (b) in oxidising condition. In case a dopant of valency higher than 3+, is introduced in the ferrite structure, the effect of

reducing atmosphere is to reduce the oxidation state of Fe^{3+} to Fe^{2+} for maintaining charge balance. The effect of oxidising atmosphere is to replace any cation to balance the charge as Fe^{3+} cannot transform to Fe^{2+} in such a case. These changes lead to change in anisotropy constants, magnetic saturation values etc.

The change in magnetic properties viz., magnetic saturation value, disaccommodation coefficient, Q-factor etc. of Mn-Zn-ferrite was studied by C. O'Hara[6] et.al. by changing the oxygen partial pressure and temperature of firing. They got best magnetic properties when the composition was close to stoichiometric composition. Slick and Blassches[7] found that the decrease of atmospheric oxygen content or increase in sintering temperature results in an weight loss due to sublimation of Zinc oxide in Mn-Zn-ferrite. This leads to the use of packing material while firing the Zinc containing ferrite samples to maintain the partial pressure of oxygen in the system at the desired level.

Substantial amount of work has been done on the ferrites particularly on Mn-Zn ferrites and Ni-Zn-ferrites due to their high industrial demands. A considerable amount of work has been done on the effect of dopants on the ferrites. The effect of Co^{2+} on magnetite has been described by Slonczewski and Bitchford et.al.

A good deal of work has been done on the effect of additives of different transition metal ions, such as Indium,

Scandium, alkali and alkaline earths, Copper, different rare earths and also on other additives.[8]

Tebble and Craik[9] reported following Gorter and Brokman that the bulk and sintered densities of Ni-Zn-ferrites increase as percentage of Zn^{2+} is increased. According to the authors, the initial permeability increases as sintered density increases but Curie temperature shows opposite behaviour.

Some work has been done so far on the effect of Titanium specially on Ni-Zn-ferrite. Gorter[10] reported the effect of Ti^{4+} on Ni-ferrites and Ni-Zn-ferrite. His range of composition was from $NiFe_2O_4$ to $Ni_{1.5}FeTi_{0.5}O_4$ and $Ni_{1.5}FeTi_{0.5}O_4$ to $NiZn_{0.5}FeTi_{0.5}O_4$ in which percentage of Titanium was fixed. He did not draw any firm conclusion regarding the position of Ti^{4+} in the lattice. Stinges[11] et.al. substituted Ti^{4+} in Mn-Zn-ferrite and have seen the effect on permeability and electrical conductivity. He found that replacing $2Fe^{3+}$ by $Ti^{4+} + Fe^{2+}$ in octahedral site of the ferrite results a strong temperature dependent positive contribution to the magnetic anisotropy. This was done under reducing condition. Syono, in magnetite, found for larger amount of Ti^{4+}, the anisotropy to become larger than 10^6 ergs/cc. This is ascribed to Fe^{2+} in A site. According to Banerjee et.al. Fe^{2+} ions occupy tetrahedral sites for most part of the solid solution series $Fe^{3+}_{2-2x}Fe^{2+}_{1+x}Ti^{4+}_{x}O_4$ and cause large anisotropy. Hoene, in Fe_3O_4, found that Ti^{4+} doping shifted the Curie point to lower temperature.[12]

According to Knowles[13] the effect of quadrivalent Ti^{4+} is to localise a Fe^{2+} ion so increasing the resistivity and decreasing the loss in Mn-Zn-ferrite. He also expected the same behaviour from Sn^{4+} but some of the effects due to this ion is in intermediate between those of ferrites substituted with Ti^{4+} and unsubstituted ferrites and some is anomalous. It was concluded that the differences in behaviour between ferrites substituted with Sn and Ti originate in the larger size of the Sn^{4+} ion.

Blasse[14] in his well known work substituted Fe^{3+} in $Me^{2+}Fe_2^{3+}O_4$ by various cations of valencies ranging from 2+ to 5+ and studied magnetic properties of those substituted ferrites. He reported the replacement of Fe^{3+} as $\frac{2}{3}Me^{2+} + \frac{1}{3}Sb^{5+}$ in his paper. He used Ni^{2+}, Mg^{2+}, Co^{2+} and mixtures of them as Me^{2+}. He could dissolve Sb^{5+} ($r = 0.62$ Å) upto 0.67 mole fraction in these ferrites but was unable to dissolve Nb^{5+} ($r = 0.69$ Å) which has largerionic radius than Sb^{5+}. He explained this insolubility to be due to absence of cation-cation bonding in case of Nb^{5+}. In the same paper he postulated the replacement of Fe^{3+} from octahedral sites by Ti^{4+} in Mg-, Co- and Li-ferrites, but in case of Ni-ferrite the partial substitution of Fe^{3+} is possible from tetrahedral position.[15] According to Gorter, the possibility of Ti^{4+} to replace Fe^{3+} is more in B site in case of $NiZn_{0.5}FeTi_{0.5}O_4$, the composition discussed earlier.[10]

The lattice constant of mixed ferrites are mostly found in good approximation by linear interpolation of the lattice constants of the constituent simple ferrites. In case of Ni-Zn-ferrites the value were studied by Guillaud[16] for the whole range of the mixture. Later this was verified by Kedesky[17] et.al. and this value was adopted by A.S.T.M.[18] Murthy[19] et.al. again studied the lattice parameter of these ferrites as a function of Zn along with magnetic susceptibilities and magnetic moments.

Saturation magnetization is one among the important properties of soft ferrites. Gorter made the extensive report[10] on this subject first and has been considered as the authority in this area. He showed the discrepancy in the magnetic saturation moment between theoretical and practical values and brought out a clear picture of it. Later on, a large number of workers have done several experiments on this property with or without any temperature variation.

Chapter 2

PRESENTATION OF THE PROBLEM

High valence cations when substituted in ferrite, is expected to cause either cation vacancies or convert Fe^{3+} to Fe^{2+} in spinel model depending on whether the atmosphere of ferritisation is oxidising or reducing. In either case there will be density changes (lattice density of powder) in the material which can be compared with accurately measured powdered densities to check the validity of the model.

Depending on the vacancy (vacant Fe^{3+} site positions) the magnetic moment of the lattice will be influenced. Estimates of magnetic saturation moment may be made on the basis of site occupancy and compared with measured values of magnetic saturation moment by magnetometer.

We have chosen a composition of 50:50 Ni-Zn-ferrite which posses maximum value of magnetic saturation moment (M_s). For this composition it was decided to do the following:

a) the measurement of lattice parameter,

b) the measurement of pycnometric density and to compare the experimen lattice density with calculated values on the basis of suitable site occupancy models due to addition of different dopants, and

c) measurement of the saturation magnetic moment by magnetometer and to explain its behaviour on the basis of proposed site occupancy model.

The dopants used were Ti^{4+}, Zr^{4+} and Nb^{5+} which have ionic radii close to that of Ni^{2+}, Zn^{2+} and Fe^{3+} so that they can substitute ions from the base Ni-Zn-ferrite.

Chapter 3

EXPERIMENTAL METHOD

3.1. Raw Materials

The raw materials used for preparation of Ni-Zn-ferrite and corresponding dopants are noted below.

	Raw materials	Grade	Maker
a)	Nickel carbonate hydroxide ($NiCO_3$, $2Ni(OH)_2$, $4H_2O$)	A.R.	Thomson and Baker Co. Ltd.
b)	Iron oxide (Fe_2O_3)	A.R.	Thomson and Baker Co. Ltd.
c)	Zinc oxide (ZnO)	A.R.	May and Baker Ltd.
d)	Titanium metal (Ti)	>99.9%	
e)	Zirconium oxide (ZrO_2)	>99.9%	
f)	Niobium oxide (Nb_2O_5)	>99.9%	
g)	Sulphuric acid (H_2SO_4)	A.R.	BDH

The above mentioned raw materials were used for sample preparation. For packing powder, Iron oxide, Nickel oxide and Zinc oxide of L.R. grade were used.

3.2. Preparation of Packing Powder

The raw materials were weighed accurately following Table 2. The weighed raw materials were mixed in an agate mortar and directly fired in an electrically heated furnace at 1250°C for 4 hours taking it in sillimanite crucibles.

3.3. Preparation of Samples

3.3.1. Mixing of raw materials - The raw materials were weighed in an electronic pan balance (Owabar, Germany) with an accuracy upto fourth figure of decimal place. They were transferred carefully in a porcelain mortar for preliminary mixing. As the raw materials were fine enough they did not require further grinding. After primary mixing the raw materials were mixed in an alumina porcelain ball mill with alumina balls for one hour with proper amount of distilled water. Finally the batch was taken out and dried.

3.3.2. Preparation of samples for determining minimum ferritisation temperature - In order to establish the minimum temperature at which complete ferritisation occurs, several pelletised samples of the batch were taken in alumina crucibles. The pelletswere completely covered with packing material upto the seam of the crucibles and were treated at 850°C, 900°C, 950°C, 1000°C, 1050°C, 1100°C, 1150°C, 1200°C and 1250°C individually for 4 hours in an electrically heated muffle furnace. The furnace was cooled slowly. The completion of ferritisation was checked by X-ray diffractograms.

3.3.3. Preparation of base material - The batch material was pressed into 1/2 inch dia. pellets. They were taken in an alumina crucible and covered with packing material. They were calcined at 800°C for 1 hour in an electrically heated

furnace. The pellets, after cooling, were ground thoroughly in an agate mortar for thorough homogenisation and again pressed into pellets. They were finally ferritised at 1250°C for 4 hours in an electrically heated muffle furnace using Platinum-Platinum 10% Rhodium thermocouple and temperature controller (Leeds and Northrup, Electromax).

3.4. Preparation of Dopant Solutions

3.4.1. Analysis - Known amounts of dopants i.e. Ti (as metal), Zr (as ZrO_2) and Nb (as Nb_2O_5) were dissolved individually in concentrated sulphuric acid (36 N) taking them in Platinum crucibles. The sulphates produced were dried at low temperatures and finally fired at 1000°C in muffle furnace for half an hour. The final weights of the materials were taken to check the complete decomposition of sulphates and stoichiometry of the oxides. The experiment was repeated.

To know the exact temperature of decomposition of sulphates, the sulphates were given for DTA analysis (Derivatograph, MOM, Hungary).

3.4.2. Preparation of dopant solutions of known concentrations - Titanium - Known amounts of the powdered Ti-metal were dissolved in 1:1 ($\frac{v}{v}$) sulphuric acid. The solutions were heated gently to increase the dissolution rate. Two solutions one of lower and other of higher concentrations were used at low and high concentrations of dopants in

samples. 50 ml solutions of both concentrations were prepared using volumetric flask.

Zirconium - Zirconium oxide (ZrO_2) was used for Zirconium. As Titanium, known weights of Zirconia were taken to prepare two solution of different concentrations. Zirconia was treated with concentrated Sulphuric acid (36 N) at about 200°C to convert Zirconia to Zirconium sulphate. The dried crystals of Zr-sulphate were dissolved in water and 50 ml solutions were prepared.

Niobium - Niobium oxide (Nb_2O_5) was used for Niobium. It was weighed and dissolved in concentrated Sulphuric acid (36 N) directly. It was strongly heated to get a clear solution and the volume was made upto 100 ml.

3.5. Dopant Addition

The exact volume of dopant solutions required for incorporating them in the base ferrite to get required amounts of dopants, were calculated.

Known amounts of green Ni-Zn-ferrite batch were taken in petridishes. Known volume of dopant solutions were added to the samples dropwise using a microburette carefully distributing it all over the sample. Care was taken so that the solution might not flow out of the powdered mass. The powders were dried gently and for larger concentrations of dopants in samples, these additions were repeated after

intermitent drying of the solution. The batches were ground in agate mortar after each addition of solution to get homogeneity of the dopants in the samples.

3.6. Heat Treatment of the Doped Samples

The doped samples were pelletised and were taken in alumina crucibles with packing material covering them. Initially they were heated at 800°C for 1 hour. For each dopant four samples of different dopant concentrations were heated altogether at a time so that they can get same heat treatments. The cooled pellet were again ground and mixed thoroughly in an agate mortar. They were again pressed into pellets and fired at 1250°C for 4 hours with packing materials covering them. The temperature of the furnace was controlled carefully using controller. The furnace was cooled slowly.

3.7. X-ray Analysis

3.7.1. To estimate the minimum ferritisation temperature - The pellets (as obtained in Section 3.3.2) were ground in an agate mortar to -200 mesh (ASTM) for X-ray study. They were taken in a X-ray sample holder of groove size 15 x 15 x 1 mm and X-ray diffractograms were taken in XRD-5 (G.E.C., England). The data were compared with the given ASTM data of the starting materials (viz. NiO, ZnO and Fe_2O_3) and for final product.

3.7.2. Characterisation of Ni-Zn-ferrite - The base ferrite pellets (as obtained in Section 3.3.3) were ground and X-ray diffractogram was taken as described in previous section. The position and intensities of the peaks were compared with given ASTM data for Ni-Zn-ferrite.

3.7.3. Trial runs of doped samples with silica - Originally it was felt that the incorporation of quartz would help to measure the relative shift of the d-values of the doped Ni-Zn-ferrites when compared to the fixed d-values of the quartz lines thus eliminating machine error. So the ground samples were mixed with 25% pure α-quartz (by weight). That gave a good sharp peak of quartz compared to that of ferrite. Attempts were made to measure the shift in 2θ values with respect to that of standard quartz. As the readings of 2θ values in the chart were not accurate so this method was given up and the point count method was adopted.

3.7.4. Point count for measuring the shift in d-values - First knowing the approximate peak positions, the powdered samples in holder were set near the peak positions and it was slowly rotated towards maximum peak position in steps and at each position the X-ray counts were noted by an automatic timer for certain periods of time. Two machines were used for this purpose: (i) Siefert (Germany) of accuracy 0.001° in 2θ values and (ii) XRD-5 (G.E.C. England) of accuracy 0.01°.

Initially to know the approximate peak positions, the angles were changed by hand in steps of 0.05° then in steps of 0.02° noting the counts for 10 seconds. Finally, the angles were changed in steps of 0.002° and the counts were noted for 60 seconds in Siefert diffractograph. Measurements for Ti-doped samples were done in this machine. In XRD-5, the angles were changed in steps of 0.05° initially noting the counts for 20 seconds and finally by 0.01° noting the counts for 100 seconds. Measurements of Zr- and Nb-doped samples were done in this machine. The XRD-5 machine needed to use because of break down of the Siefert machine.

The d-values were calculated using Bragg's formula i.e. $\lambda = 2d \sin\theta$, where λ is the wave length of X-ray used and θ is the peak angle in degree.

The d-values calculated were used to find out the lattice parameter, a, as

$$a = d(h^2 + k^2 + l^2)^{1/2}$$

where hkl are the indices of the X-ray reflecting plane.

These a values were plotted with Nelson-Riley function, which is given by

$$f(\theta) = \frac{1}{2}\left(\frac{\cos^2\theta}{\sin^2\theta} + \frac{\cos^2\theta}{\theta}\right) \qquad \text{(See Appendix)} \qquad (1)$$

The curve of $f(\theta)$ verses lattice parameter (a) should be a straight line and the extrapolated value of 'a' corresponding to $f(\theta) = 0$ gives the accurate value of 'a'.

3.8. Density Measurement

The density of samples were determined using pycnometer bottle. The sizes of two bottles used were of 1 ml volume and of 2.5 ml volume. The method used is same as that of specific gravity bottle. The density of the sample is given by

$$\rho = \frac{w_2 - w_1}{(w_4 - w_1) - (w_3 - w_2)} \times \frac{w_4 - w_1}{w_5 - w_1} \times \rho_t$$

where, w_1 = weight of the empty bottle,

w_2 = weight of bottle + sample (about 1/3 filled)

w_3 = weight of bottle + sample (as before) + liquid (filling rest of the bottle)

w_4 = weight of the bottle + liquid (filling the bottle)

w_5 = weight of the bottle + water (filling the bottle), all are at room temperature,

and ρ_t = density of water at room temperature, in gms/ml.

Initially to establish the accuracy of the method crushed single crystal alumina powder was taken whose density was measured using distilled water. For the samples, the densities were measured using A.R. Grade Toluene.

Standard deviation in densities of each sample was calculated using the formula

$$\text{Standard deviation, } s = \left(\frac{\Sigma(\rho_i - \bar{\rho})^2}{n}\right)^{1/2}$$

where $\bar{\rho}$ is the average density and n is the number of readings taken.

3.9. Magnetic Measurements

Only the saturation moment of the samples were measured. Small known amounts of powdered samples were taken. P.V.A. solution in water of known concentration was added dropwise to the samples and mixed thoroughly. The samples were dried when required to keep the moisture content at proper consistency for pressing. Two pellets were prepared for each samples in a 3 mm dia. die.

The weighed pellets were kept in the magnetic field of a parallel field vibrating magnetometer (model 150 A EG & G, PARC, U.S.A.). In this magnetometer the samples are kept in vibration in a vertical direction while the magnetic field acts in horizontal direction. The induced a.c. field produced by the sample in a pair of secondary coils placed on both sides of the sample is amplified and compared with the signal produced by a standard magnet giving rise to an output signal which is proportional to the magnetic moment of the specimen.

To know the approximate saturation moment, magnetic fields were increased gradually upto 6.5 K.Oes and the magnetic moments were noted for the base sample. For other samples saturation magnetic field was applied directly and the magnetic moments were noted.

The saturation magnetic moment of a sample is given by either by $\sigma_s = \frac{\sigma}{m}$ emu/gm, where σ is the observed saturation magnetic moment of the sample and m is the mass of the magnetic material or by $4\pi M_s$ emu/cc, where $M_s = \sigma_s \times \rho$ emu/cc.

Chapter 4

RESULTS AND DISCUSSION

4.1. Raw Materials

Batches were prepared for both the samples as well as packing materials following Table 2. Total batch of 800 gms for samples and 500 gms for packing materials were prepared.

4.2. Packing Material

As Zinc has low vapour pressure so at high temperature ZnO sublimes and decomposes as

$$ZnO\ (s) \quad — \quad Zn\ (g) + \frac{1}{2}\ O_2\ (g)$$

We know from Ellingham diagram the partial pressure of Oxygen at 1250°C is 10^{-12} atm. So to prevent the expulsion of Zinc from the sample proper Oxygen partial pressure has to be maintained by covering the samples with suitable material. If pure Zinc oxide is used around the samples then the high concentration of Zn will lead to diffusion of Zinc in the sample and hence the composition of samples will change. So, usual practice is to use a material having same Zinc content as the sample. It provides sufficient partial pressure of Zinc as required for the samples to stop expulsion of Zinc. The crucibles were also closed at the top.

4.3. Preparation of Raw Materials

4.3.1. Mixing of raw materials - Mixing was done in alumina porcelain ball mill for 1 hr. The short time of mixing was chosen to minimise contamination from the balls and walls of the ball mill. Previous worker[20] reported the contamination level to be about 0.1% per hour in alumina porcelain ball mill. Grinding and mixing were done mainly in agate mortar to avoid contamination.

4.3.2. Preparation of samples for determining minimum ferritisation temperature - The furnace used for firing the samples was electrically heated Silicon Carbide furnace the temperature of which was automatically maintained using temperature controller (Leeds and Northrup, Electromax). The temperature was controlled in the range of $\pm 5^{\circ}C$. About 3 grammes of base sample was taken for firing at different temperatures for 4 hours. The samples were pelletised to enhance reaction.

4.3.3. Preparation of base material - Initial firing at 800°C is for decomposition of the Ni-salt to oxide of sub-micron size and the following mixing in agate mortar increases homogeneity of the material. This also increases quicker ferritisation at 1250°C.

4.3.4. Addition of dopants - At low dopant percentages (viz. 0.2%) the volumetric proportion of dopant is very low

than the base material so mixing the dopants to have a homogenised mass is a problem. If the dopants are used in powder form, due to the relatively higher particle sizes of the dopants, homogenisation by sintering is not possible and it requires repeated sintering and grinding to have a better product which brings forth impurities. So solution method of addition of dopants was adopted which enables fine dopant particles on decomposition and thus a more homogenised product.

Attempts were made to dissolve the dopants in acids. Zirconium oxide and Niobium oxide do not dissolve in Hydrochloric acid or Nitric acid. They dissolve in Phosphoric acid, Hydroflouric acid and Sulphuric acids. Zirconium and Niobium phosphates decompose at high temperatures and hence this method of addition of dopants was rejected and as flourides volatilise at lower temperatures, so it was also rejected. The sulphates of them decompose at 798°C and 766°C respectively (determined by D.T.A. and T.G.A. methods). As Titania is soluble in Sulphuric acid to only a small extent and has similar problems as with other acids, so Ti-metal was used as the raw material for Titanium doping. Ti-sulphate decomposes at 708°C (determined by D.T.A. and T.G.A. methods). The dissolution process with hot sulphuric acid is a problem due to atmosphere pollution with the acid vapour. Use of acid fume chamber will reduce the problem.

The dopant solutions were added into the samples using a microburette which can read upto 0.05 ml. As the

batch materials taken were 3.5 gms each, it was not possible to add dopant solution more than 3 ml at a time. For higher concentration of dopants repeated additions after drying were done to achieve required dopant concentrations. The data is shown in Table 3 for Titanium. Same addition methods were applied for Zirconium and Niobium.

4.4. X-ray Analysis

4.4.1. To estimate the minimum ferritisation temperature - The X-ray diffractograms were taken for each samples fired at different temperatures ranging from 850°C to 1250°C. The peaks in the diffractograms were compared with starting materials as Zinc oxide, Nickel oxide and Iron oxide (Fe_2O_3) and with final products, Ni-Zn-ferrite. The decrease in the Iron oxide peaks with increase in Ni-Zn-ferrite peaks were prominent with the increase in firing temperature. At 1150°C the most intense peak of Fe_2O_3 was completely disappeared together with the clear and sharp appearance of prominent peaks of Ni-Zn-ferrite. At this temperature there was no evidence of NiO and ZnO. The ferritisation temperature was selected to be 100°C higher i.e. 1250°C for complete ferritisation.

4.4.2. Characterisation of Ni-Zn-ferrite - The results of the X-ray diffractograph of base Ni-Zn-ferrite is given in Table 4. This is compared to the given A.S.T.M. values which

show a close match with the exception of the second and the fourth highest peak intensities which are low in the present case. A few X-ray peaks were not found in our sample. This may be due to high noise production by our small sample holder due to scattering from the perspex surface. The hkl values as given by A.S.T.M. were adopted and the same for only the last peak was self indexed.

4.4.3. Trial runs of doped samples with silica - With Silica X-ray diffractograms were taken for Titanium and Niobium doped ferrites in XRD-5. The chart did not give accuracy upto required level and also the variation of d-values were random so this method was rejected and point count method was adopted.

4.4.4. Point counts for measuring the shift in d-values - The method for finding out the actual peak angles from point counts are shown in Figure 2 for Ti-doped ferrite and the data is given in Table 5.

4.4.5. Estimation of lattice parameter - Accurate determination of lattice parameter is discussed in Appendix. The results of estimation of d, hkl, lattice parameter and corresponding Nelson-Riley functions are indicated in Table 6. Figures 3, 4 and 5 show the plots of lattice parameter vs. Nelson-Riley function for only three highest angle values. The remaining lower angle values gave

erroneous results as they are in a nonlinear part of the curve and these points are rejected. The results of lattice parameter values are given in 10th column of Table 6 which can be read from the Y-axis from the Figures 3, 4 and 5 at $f(\theta) = 0$. Standard deviations for lattice parameters were not analytically determined because it is evident from the plotted figures that these values would be low and below $\pm$ 0.0004. The standard deviation from Figures 4 and 5 are still lower.

Figures 6, 7 and 8 show the variation of lattice parameter of the ferrite composition doped with TiO_2, ZrO_2 and Nb_2O_5 respectively. It is seen in Figure 6 that there is a drop in lattice parameter at low percentages of TiO_2 upto 0.8907% followed by increase at higher percentages with decreasing slope. Literature reports solubility of Ti in Ni-ferrite upto $Ni_{1.5}FeTi_{0.5}O_4$ and in Ni-Zn-ferrite upto $NiZn_{0.5}FeTi_{0.5}O_4$ as reported by Gorter[10]. Our Ti-content in Ni-Zn-ferrite was upto 0.4217 mole Ti per mole of Ni-Zn-ferrite.

Figures 7 and 8 show that there is an increase in lattice parameter upto 3.40% dopant level for ZrO_2 and 0.89% for Nb_2O_5 after which they are almost constant showing immiscibility of these dopants in Ni-Zn-ferrite. As reported by Blasse[15] that Nb_2O_5 is completely insoluble in Ni-ferrite is probably due to the lack of sufficient accuracy in his measurements which was reported upto 3rd decimal place.

We have measured lattice parameter upto 4th decimal place and found small degree of solubility of Nb_2O_5 in Ni-Zn-ferrite.

The small variation in lattice parameter of same Ni-Zn-base ferrite as shown in Figure 6 (a = 8.3974 Å) and in Figures 7 and 8 (a = 8.3936 Å) is probably due to measurement in two different machines as compared to 8.399 Å as reported by A.S.T.M.[18].

4.5. Density

Standard deviations as shown in Figures 6, 7 and 8 is about ±1%. It is possible for pycnometer readings to be more accurate and reported values of 0.1% is quoted. In our method use of vacuum and low surface tension liquid although expected to produce higher accuracy still the results are not good. This might be improved by using a larger bottle (5 ml or 10 ml) with larger sample amounts.

In literature the reported density values of Ni-ferrite is 5.38 gms/ml and that of Zn-ferrite is 5.33 gms/ml. Taking arithematic mean of the two, the density of $Ni_{0.5}Zn_{0.5}Fe_2O_4$ comes to be 5.355 gms/ml whereas we have got the value to be 5.2567 gms/ml. Starting with the instrument, same high value in standard deviation was observed for ground single crystal alumina. Table 7 shows the densities of all compositions and Figures 6, 7 and 8 show the plots of density variation versus dopant content. Densities were calculated following the formula:

Calculated density, ρ_i, gms/ml =

$$\frac{\text{weight contributed by the elements in the formula} \times 8}{(\text{measured lattice parameter})^3 \times \text{Avogadro number}}$$

(since, 8 formulae form the unit cell).

For $Ni_{0.5}Zn_{0.5}Fe_2O_4$, the density is, calculated as,

$$\rho_i = \frac{237.5 \times 8}{(8.3974 \times 10^{-8})^3 \times 6.03 \times 10^{23}} = 5.317 \text{ gms/ml}$$

Density by mixture rule was calculated by taking the weighed average of densities of Ni-Zn-ferrite and the corresponding oxide. For 0.89% TiO_2 the density of the mixture is given by,

$$\frac{1 \text{ gm ferrite} + 0.0089 \text{ gm } TiO_2}{\text{volume of ferrite} + \text{volume of } TiO_2} = \frac{1 + 0.0089}{\frac{1}{5.317} + \frac{0.0089}{4.26}}$$

$$= 5.305 \text{ gms/ml}$$

The standard deviations for the measured densities are also indicated in the plots.

For Titanium doped ferrite, the measured density increases upto 0.2646% TiO_2 and subsequently falls monotonically after that. Although the standard deviation is high and the observed rise may appear to be spurious at first sight, the rise may be connected with fall of corresponding lattice parameter as shown in the same figure. The matter is discussed in the following pages.

Figure 7 shows the density of Zirconium doped ferrite to be dropping sharply followed by rise and then gradual fall up. Similarly, the density of Niobium doped ferrite (figure 8) falls down sharply and then rises rapidly at higher percentages.

More comments in this aspect are given in later discussions.

4.6. Magnetic saturation moment

The details of magnetic saturation moments are given in Tables 8 and 9 and in Figures 9 and 10. In Table 8, the nature of variation of magnetic moment with applied magnetic field is shown for the base sample. This is just to know the field required to get saturation magnetic moment. Due to low capacity of the magnetometer, it was not possible to go beyond 6.5 K.Oes where the magnetic moment of the sample is seen to rise though at a very slow rate. Later on, the magnetic moments of all the samples were taken at 6.5 K.Oes and are considered to be the saturation magnetic moments.

Table 9 and Figures 9 and 10 show the nature of variation of magnetic saturation moments with dopant concentrations. The nature of all the curves are essentially same; all of them have derepressions at low percentage of dopant concentrations. The curves then rise a bit, level off and come down at higher percentages of dopants. The depression is highest in case of Zirconium dopant followed by Niobium (Figure 10) and Titanium (Figure 9) dopants. The fall off portion is greatest in case of Titanium doped samples which can be explained by solid solubility of Titanium at higher percentages and is discussed in the following chapter. The effect of Zirconium and Niobium are not so high as Titanium and that is due to immiscibility of them in Ni-Zn-ferrites at higher percentages. All these are discussed in the following chapter.

Theoretical magnetic saturation values (for Titanium doping, shown in Figure (9)) were calculated taking help of Figures 1(a) and (b) and Figure (11). Figure 1(a) shows the variation of theoretical and measured magnetic saturation moments of Ni-Zn-ferrites with mole fraction of Zinc. Figure 1(b) shows the variation of magnetic saturation value (emu/gm.) of 50:50 Ni-Zn-ferrite with temperature. From this graph temperature correction for magnetic saturation moment values can be made. Figure (11) is actually derived from Figure 1(a). Along x-axis, the ratio of Fe^{3+} in B sites and total Fe^{3+} ions plotted following formula, $(Zn_xFe_{1-x})^A(Ni_{1-x}Fe_{1+x})^B O_4$. In y-axis, the ratio of measured and theoretical magnetic saturation moments are plotted following Figure 1(a). Thus knowing theoretical magnetic saturation value, the experimentally observed values can be calculated for certain Fe^{3+} in B sites.

For $Ni_{0.5}Zn_{0.5}Fe_2O_4$, the experimental magnetic saturation moment can be calculated as follows:
The formula can be written as, $(Zn_{0.5}Fe_{0.5})(Ni_{0.5}Fe_{1.5})O_4$.
Here,

$$\frac{Fe^{3+}(B)}{Fe^{3+}(A)+Fe^{3+}(B)} = \frac{1.5}{2} = 0.75.$$

The theoretical magnetic saturation moment is,

$$((0.5x2 + 1.5x5) - 0.5x5)x8\ \mu_B = 48.0\mu_B$$

∴ Experimental saturation moment is

$$48.0x0.85 = 40.8\ \mu_B \text{ (from Figure 11)}$$

$$= 40.8 \times 1.1653 \times 10^{-29} \text{ (Wb-m)} \times \frac{10^{30}}{694.66 \text{ (m}^3\text{)}} \times 7.96 \times 10^{2} \text{ Gauss}$$

$$= 544.7 \text{ Gauss} = \frac{544.7}{5.32} \text{ Gauss cm}^3\text{/gm.} \quad \left(\text{density} = 5.32 \frac{\text{gms}}{\text{ml}}\right)$$

$$= 102.4 \text{ Gauss cm}^3\text{/gm or emu/gm. at } 0^\circ\text{K.}$$

At room temperature (say, 25°C) the value is, $102.4 \times \frac{75}{115}$ emu/gm

$= 66.78$ emu/gm. (using Figure 1(b)).

Chapter 5

GENERAL DISCUSSION

5.1. Density and Lattice Parameter Changes

When a cation of different valency is introduced in another compound, the effect is creation of extra positive charge or its defficiency according as whether the incoming cation has higher or lesser valency. In case of higher valency cations the extra charge is balanced either by expulsion of cations or by changing the valency to lower state of cations.

Let us take an example of replacement of Fe^{3+} by Ti^{4+} in Ni-Zn-ferrite as in our case. As the partial pressure is expected to be higher than that corresponding to the fully oxidising condition the charge balences as $Ti^{4+} + Fe^{2+} \rightleftharpoons 2Fe^{3+}$ i.e. $Fe^{3+} \rightarrow Fe^{2+}$ is not possible. So the conservation of charge can only be explained by expulsion of cations (divalent and or trivalent) due to introduction of Ti^{4+}. We have postulated four different models to explain this phenomenon assuming the proportion of Ni : Zn to be always constant as the base material has been prepared in stoichiometric proportion.

The four models may be summarized as below:

I) the dopant exclusively replaces Fe^{3+} which goes out as insoluble α-Fe_2O_3,

II) the dopant exclusively replaces Fe^{3+} which goes out as soluble γ-Fe_2O_3 phase,

III) divalent cations go out and precipitates as separate oxides;

IV) dopant oxide contributes to an increased lattice due to addition of oxygen and divalent and trivalent cations are proportionally removed;

I) Fe^{3+} goes out and forms α-Fe_2O_3 which is not soluble in the ferrite structure.

The equation is,

$$Ni_{0.5}Zn_{0.5}Fe_2O_4 + 3xTiO_2 \rightleftharpoons Ni_{0.5}Zn_{0.5}Fe_{2-4x}Ti_{3x}O_4 + 2xFe_2O_3$$

Here, Fe^{3+} vacancies are created in the structure. According to this model, as if the 2x moles of α-Fe_2O_3 are in with the ferrite and the density can be calculated accordingly.

II) Fe^{3+} comes out and forms γ-Fe_2O_3 structure which is again soluble in the spinel formula and can be represented as,

$$Ni_{0.5}Zn_{0.5}Fe_2O_4 + 3x\ TiO_2 \rightleftharpoons Ni_{0.5}Zn_{0.5}Fe_2Ti_{3x}O_{4+6x}.$$

The right hand side of this equation can be represented as,

$$Ni_{\frac{0.5x4}{4+6x}}\ Zn_{\frac{0.5x4}{4+6x}}\ Fe_{\frac{2x4}{4+6x}}\ Ti_{\frac{3x\ x4}{4+6x}}\ O_{\frac{(4+6x)x4}{4+6x}}$$

or,

$$Ni_{\frac{1}{2+3x}}\ Zn_{\frac{1}{2+3x}}\ Fe_{\frac{4}{2+3x}}\ Ti_{\frac{6x}{2+3x}}\ O_4.$$

The density of this structure is given by,

$$\rho = \frac{\text{mass of the formula x 8}}{(\text{observed lattice parameter})^3 \text{x Avogadro number}}$$

III) The divalent cations in the lattice go out as a separate phase forming oxides as,

$$Ni_{0.5}Zn_{0.5}Fe_2O_4 + x\ TiO_2 \rightleftharpoons Ni_{0.5-x}Zn_{0.5-x}Fe_2Ti_xO_4 + xNiO + xZnO$$

i.e. one divalent cation vacancy is created for one Ti^{4+}.

The density of the structure is given by mixture rule.

IV) Vacancies are created in the cation sites maintaining Ni, Zn : Fe ratio constant.

Assuming four O^{2-} ions per formula and $xTiO_2$ enters in it, the equation can be represented as,

$$Ni_{0.5}Zn_{0.5}Fe_2O_4 + xTi \rightleftharpoons Ni_{0.5}Zn_{0.5}Fe_2Ti_x\ O_{4+2x}$$

The right hand side of the formula can be represented as,

$$Ni_{\frac{0.5x4}{4+2x}}\ Zn_{\frac{0.5x4}{4+2x}}\ Fe_{\frac{2x4}{4+2x}}\ Ti_{\frac{4x}{4+2x}}\ O_{\frac{(4+2x)x4}{4+2x}}$$

or,

$$Ni_{\frac{1}{2+x}}\ Zn_{\frac{1}{2+x}}\ Fe_{\frac{4}{2+x}}\ Ti_{\frac{2x}{4+2x}}\ O_4 .$$

The density of the structure is given by,

$$\rho = \frac{\text{mass of the formula x 8}}{(\text{observed lattice parameter})^3 \text{ x Avogadro number}} .$$

Besides these models another model can be considered for density. If the cation is not soluble in the structure, the net density of the mixture is given by the weight proportion of the densities of two phases. The density is given by,

$$\rho = \frac{\text{weight of ferrite + weight of dopant added}}{\text{volume of the ferrite + volume of the dopant added}} ,$$

$$= \frac{1+y}{\frac{1}{\rho(\text{ferrite})} + \frac{y}{\rho(\text{dopant oxide})}} ,$$

where 'y' is the weight fraction of dopant oxide added.

In the above discussed models, none of models (I), (II) and (III) are probable because Ni and Zinc are in stoichiometric proportion and dopants are added separately. It is most probable to consider that the dopants will create cation vacancies in stoichiometric proportion. Hence model (IV) is used to calculate density is all cases. In the absence of solubility, the mixture model would be appropriate.

Considering model (IV) for theoretical density, we have an illustrative example for 0.4217 mole fraction of Titanium. The formula can be written as,

$$Ni_{\frac{1}{2+0.4217}}\ Zn_{\frac{1}{2+0.4217}}\ Fe_{\frac{4}{2+0.4217}}\ Ti_{\frac{2\times0.4217}{2+0.4217}}\ O_4.$$

The molecular weight of this structure

= (molecular weight of the formula) x 8, as 8 such formulae give an unit cell,

= 233.79 x 8 = 1790.3 gms.

The measured lattice parameter of the structure is a = 8.405 Å.

Therefore, density of this structure is,

$$= \frac{\text{weight of unit cell}}{a^3 \times 6.03 \times 10^{23}}$$

$$= \frac{1790.3}{(8.405)^3 \times (10^{-8})^3 \times 6.03 \times 10^{23}} \text{ gms/ml.} = 5.000 \text{ gms/ml.}$$

For Zr^{4+} ion, the structure is same as Ti^{4+} but for Nb^{5+} it is different and is given by,

$$Ni_{\frac{2}{4+5x}}\ Zn_{\frac{2}{4+5x}}\ Fe_{\frac{8}{4+5x}}\ Nb_{\frac{8x}{4+5x}}\ O_4.$$

The calculated densities are plotted in Figure 6 for Titanium and is found to follow the general trend of experimental value of pycnometric density except at very low percentages. The experimental density values are seen to rise upto 0.2646% TiO_2 and then falls monotonically. The lattice parameters as determined by X-ray technique also are seen to fall followed by monotonic rise.

When smaller size ions enter into the structure (viz. Ti^{4+} (0.61 Å) for Fe^{3+} (0.65 Å)), it is possible that the lattice parameter may fall and at the same time when cation vacancies are created the lattice parameter may increase (since vacant sites cause neighbouring ions to repel each other). The two opposite tendencies may cause a minimum in the lattice parameter versus dopant curve. Such a drop in the lattice parameter would result in corresponding increase in density which can be estimated from the mass of the unit cell. However, in this case, the observed rise is about 20 times that is accountable by lattice parameter drop. It may however be noted that the pycnometric density values are not that accurate as shown by the standard deviation for the point at 0.2646% TiO_2 level to be quite large. Therefore, it is possible that the measured density rise may not be so high and may be closer to that which is accountable by lattice parameter at that point. After 0.8907% TiO_2 in Ni-Zn-ferrite the monotonic lattice parameter is observed with decreasing slope. The density curve

after, this mole fraction of Ti^{4+} is seen to go parallel with the calculated mixture density curve. These tell the decrease in solubility of Titanium at higher percentages (above 0.8907 mole fraction). Blasse[14] also observed a monotonic increase in lattice parameter.

Following Blasse[14] the expansion in lattice parameter by adding 1.0mole Titanium is 0.01% both in $Co_{1+t}\ Fe_{2-2t}\ Ti_t O_4$ and $Mg_{1+t}\ Fe_{2-2t}\ Ti_t O_4$ ferrites, where as in our case it is only. 0.002% per 1 mole of Titanium. This difference in expansion in the case of Blasse is due to the fact that,

a) for every Ti^{4+} entering, one Co^{2+} or Mg^{2+} enters and $2Fe^{3+}$ leave as, $Ti^{4+} + (Mg, Co)^{2+} \rightarrow 2Fe^{3+}$, leaving no physical vacancy whereas in our case, for every Ti^{4+} entering, one Fe^{3+} and one-half divalent cation go out as, $Ti^{4+} \rightarrow Fe^{3+} + \frac{1}{2}(Ni+Zn)^{2+}$, leaving a half of a vacancy and,

b) the size of the second ion entering with Ti^{4+} is Co^{2+} (0.74Å) or Mg^{2+} (0.72 Å), is larger compared to the Fe^{3+} ion leaving. Both of these contribute to large difference in the lattice expansion. At high percentages of TiO_2 addition the nature is similar to those reported in literature.

In the X-ray diffractogram the maximum peak of ZrO_2 (bedeleyite) is seen to be present at 14.19% ZrO_2 doped ferrite. The peak hight is 6% compared to that of maximum peak of Ni-Zn-ferrite.

Zirconia shows solubility upto 3.40% in Ni-Zn-ferrite which is observed by continuous variation in lattice parameter

with percentage ZrO_2 addition. After this level the insolubility is reflected by the constancy of lattice parameter. It can thus be easily reported that solubility of ZrO_2 is in between 0.8864% and 3.4031% in Ni-Zn-ferrite.

The increase in the lattice parameter due to addition of Zr^{4+} ion can be explained with the same model as Ti^{4+}. It is observed that the net increase in the lattice parameter in this case is higher than that due to the addition of TiO_2, upto 3.40%. This can be explained on the basis of larger ionic radius of Zr^{4+} (0.72 Å) than Ti^{4+} (0.61 Å) and hence the effect is proportionally larger in case of ZrO_2.

Niobium shows same behaviour in lattice parameter change as Zirconium. Only difference is that Niobium has lesser solubility, upto 0.8864% Nb_2O_5. The net increase in lattice parameter is of the same order of magnitude as Ti^{4+} and is possible as they have close ionic radii values (Nb^{5+} 0.64 Å).

In case of ZrO_2 doping the observed density change flattens off almost at the same point where lattice parameter levels which is expected (Figure 7). The slight decrease in density values at this range perhaps be accounted for error in density measurement which is clear from the large value of standard deviation. The density in this range should follow a mixture rule. The accuracy of pycnometric determination being not very high it is possible that a monotonically increasing density versus percentage Zirconia addition curve ~~which~~ will be in line with mixture rule. At the initial part of the

density curve, the reduction in observed density is from 5.2576 gms/ml. to 5.1377 gms/ml. where as, calculated values based on model (IV) is from 5.322 gms/ml. to 5.316 gms/ml. at a dopant concentration of 0.0231 mole fraction. The observed value again rises after this fall; the calculated value would show a fall but with a decreasing slope at higher percentages.

Niobium had been reported by earlier workers[16] to be totally insoluble in cobalt and Magnesium ferrites, but in our case it is clearly seen that the solubility (Figure 8) of Niobium exist in Ni-Zn-ferrite. The density of the doped ferrite also drops accordingly, although not proportionately upto the maximum solubility limit (observed drop is from 5.2576 gms/ml. to 5.077 gms/ml. and calculated drop is from 5.322 gms/ml. to 5.313 gms/ml. at 0.0012 mole fraction Nb^{5+}) and then unexpectedly it rises at higher percentages of Nb_2O_5. The dotted curve shows the variation of calculated density. The increase in density of the doped ferrite, instead of decrease, probably can be best explained by the variation of valency change of Niobium easily. Literature[21] tells the variation of densities of oxides to be from 4.47 gms/ml. to 7.3 gms/ml. for Nb^{5+} to Nb^{2+}. Thus in our case Niobium probably changes its valency to lower value and hence the density of the mixture is seen to rise. However, the reasons for such change in valency can not be explained easily.

5.2. Magnetic Saturation Moment

The curves shown in Figure 9 are already described. The essential feature of these curves are sudden drop in magnetic saturation moment value followed by increase, flattening and drop. In case of Titanium the drop is greatest compared to the other two and is due to its solubility at higher percentages. The reason of such behaviour is proposed in later portion.

For Zirconium and Niobium the effect on magnetic properties can be considered upto their solid solubility limit. Beyond this the nature of the curves will be determined by mixture rule.

Possible site occupancy for the cations: -

Broadly speaking the following site occupancies can be thought of. In actual case, however, a single one of them may not be effective throughout the whole range of solid solution when the dopant is introduced. The net saturation moment could be result of one or more of these modes acting simultaneously.

Models: -

i) All of the dopant cations go in A sites, Fe^{3+} ions are removed from A sites and corresponding Ni^{2+} and Zn^{2+} ions removed from B sites and A sites respectively.

For Ti^{4+} the basic equation of charge balance is,

$Ti^{4+} \rightleftharpoons Fe^{3+} + \frac{1}{4} Zn^{2+} + \frac{1}{4} Ni^{2+}$, as discussed earlier.

Following this equation, and model IV of density we can arrange the spinel structure as,

A site: $Zn_{\frac{4x.5}{4+2x} - \frac{4x\frac{x}{4}}{4+2x}}\ Fe_{\frac{4}{4+2x} - (\frac{2}{4+2x} - \frac{4x\frac{x}{4}}{4+2x})}\ Ti_{\frac{4x}{4+2x}}$

B site: $Ni_{\frac{4x.5}{4+2x} - \frac{4x.5x\frac{x}{4}}{4+2x}}\ Fe_{\frac{4}{4+2x} + \frac{2}{4+2x} - \frac{x}{4+2x}}$

anions: O_4.

and the saturation magnetic moment is given by, $M = |M_B - M_A|$.

Here, $M_A = \frac{1}{4+2x}(4 - 4x - 2 + x)x5$, due to Fe^{3+} only

$$= \frac{10 - 15x}{4 + 2x}\ \mu_B$$

and $M_B = \frac{1}{4+2x}(2-x)x2$ (due to Ni^{2+}) + $\frac{1}{4+2x}(4+2-x)x5$ (due to Fe^{3+})

$$= \frac{34 - 7x}{4 + 2x}$$

$$\therefore\ M_s = \frac{1}{4+2x}(34-7x - 10+15x) = \frac{12+4x}{2+x} \quad \ldots \quad (2)$$

This shows a small negative slope of $\frac{4x}{2+x}$ when plotted with M_s.

ii) All of the dopant cations go in B sites and Fe^{3+} go out from B sites as well as Ni^{2+} and Zn^{2+} from B and A sites respectively.

Using the same two equations we can write the spinel structure as,

A site: $Zn_{\frac{2}{4+2x} - \frac{x}{4+2x}}\ Fe_{\frac{4}{4+2x} - \frac{2}{4+2x} + \frac{x}{4+2x}}$

B site: $Ni_{\frac{2}{4+2x}} - \frac{x}{4+2x}\ Ti_{\frac{4x}{4+2x}}\ Fe_{\frac{4}{4+2x} - \frac{4x}{4+2x} + \frac{2}{4+2x} - \frac{x}{4+2x}}$

anions: O_4

The magnetic moments of sites are given by;

$$M_A = \frac{1}{4+2x}(4-2+x)x5 = \frac{2+x}{4+2x}x5 \text{ due to } Fe^{3+}$$

and

$$M_B = \frac{2-x}{4+2x}x2 \text{ due to } Ni^{2+}$$

$$+ \frac{1}{4+2x}(4-2x+2-x)x5 \text{ due to } Fe^{3+} = \frac{34-27x}{4+2x}$$

$$\therefore M_s = |M_B - M_A| = \frac{1}{4+2x}(34-27x-10-5x) = \frac{12-16x}{2+x} \quad \ldots \quad (3)$$

This shows a negative slope of $\frac{16x}{2+x}$ with M_s i.e. the magnetic saturation value decreases with increase in tetravalent dopant content.

In this model the ratio of $\frac{Fe_B}{Fe_A+Fe_B}$ is given by,

$$\frac{Fe_B}{Fe_A+Fe_B} = \frac{\frac{4}{4+2x} - \frac{4x}{4+2x} + \frac{2}{4+2x} - \frac{x}{2+2x}}{(\frac{4}{4+2x} - \frac{4x}{4+2x} + \frac{2}{4+2x} - \frac{x}{4+2x}) + (\frac{4}{4+2x} - \frac{2}{4+2x} + \frac{x}{4+2x})}$$

$$= \frac{6-5x}{8-4x}. \quad \ldots \quad (4)$$

iii) The dopant cations go to both the A and B sites equally replacing Fe^{3+} equally from both the sites along with Ni^{2+} and Zn^{2+} accordingly.

The effect of this type of structure will be just mean of the effects of two previous models, described.

It is expected from the model (ii) calculations that the theoretical curve of saturation magnetic moment to go down fast, but it can not explain the sudden drop, subsequent rise and fall. From the expressions for model (i) the magnetic saturation moment goes down slowly with dopant percentage and for model (iii) it goes down moderately with dopant concentration which can not explain the drastic fall of magnetic saturation value and hence they are less important.

According to Gorter[22] Ti^{4+} ion is expected to go to the B sites when substituted, although under certain conditions he has shown that a certain fraction of Ti^{4+} goes to A sites. We have seen, however, from calculations assuming A site substitution, that, the moment falls slowly with increase in dopant content which is ~~quite~~ in contrary to the expected observations. So from both grounds, A site occupancy for the Ti^{4+} may be ruled out.

Calculations on the basis of model (ii) and equation (3) show that for 0.0079 mole Ti^{4+} per mole ferrite, the percent drop in saturation moment value is about $\frac{6-5.91}{6} = 1.5\%$ where as observed drop from Figure 9 is $\frac{71.44-67.68}{71.44} = 5.12\%$. Similar calculations made by equation (3) can show the drop in magnetic saturation moment values for Zr^{4+} and Nb^{5+} to be much less than the observed values from Figure 9.

The sharp drop in all the three cases is not explainable but it is possible to postulate, after this drop that the rise may be due to A site occupancy by Ti^{4+}.

A different idea may be postulated in this connection which is as follows:

a) At very small percentages of solid solution some unexplainable strong effect is acting to depress the saturation moment very sharply.

b) However, super-imposed on this effect the normal effect of a combination of A site occupancy at the early stages by which saturation moment rises to some value followed by site occupancy at the later stages, can explain the small rise of saturation moment (after the early drop)followed by a fall off.

For Titanium, at higher percentages, the behaviour can be explained on the basis of calculated values for magnetic saturation moments. The dotted curve is theoretical and is drawn using the equations (3) and (4). For example at 0.1169 mole fraction Titanium, the magnetic saturation value at room temperature is calculated to be 57.50 emu/gm. which is smaller than the observed value, 68.20 emu/gm. This discrepancy goes on increasing at higher concentrations of TiO_2. Such higher observed values probably can be explained considering decrease in solubility of the Ti^{4+} at higher percentages which increases the net magnetic saturation moment value by a small extent.

After the solid solution range is completed for Zr^{4+} and Nb^{5+} doped samples the magnetic saturation value can be explained by mixture rule. Calculated magnetic saturation

moment, based on arithmatic proportion of the saturation moments of ferrite and nonmagnetic dopant oxides, comes to be 54.01 emu/gm, compared to observed value of 53.88 emu/gm, at 0.3696 mole fraction Zr^{4+} and is quite consistent. For Nb^{5+} at 0.0188 mole fraction the calculated value comes to be 55 emu/gm, compared to observed value of 59.46 emu/gm, which also agrees well with the model.

Chapter 6

SUMMARY AND CONCLUSIONS

The basic Ni-Zn-ferrite material was doped with Ti^{4+}, Zn^{4+} and Nb^{5+} ions as sulphate solutions to a limit of 0.4217 mole fraction, 0.3696 mole fraction and 0.0188 mole fraction for Ti^{4+}, Zr^{4+} and Nb^{5+} respectively.

Point count methods in conjunction with X-ray diffractometer was used for lattice parameter determination. Accurate values were estimated by extrapolating from standard Nelson-Riley function as lattice parameter curves.

Pycnometric densities were determined for the powdered and doped ferrite using Toluene as the liquid.

Vibrating magnetometer was used to determine the saturation magnetic moment at a maximum field of 6.5K.Oes.

The lattice parameter for the base Ni-Zn-ferrite was estimated to be 8.3974 Å as against A.S.T.M. value of 8.399 Å.

For Ti^{4+} doped samples the lattice parameter drops sharply followed by monotonic rise to the maximum of Ti^{4+} used but with decreased solubility. The measured density showed a sharp rise almost against corresponding sharp fall of lattice parameter. The density then decreases monotonically almost following the model in which Ti^{4+} ~~in~~ replaces one Fe^{3+} and one from the both Ni^{2+} and Zn^{2+} and finally at higher percentages the density follows mixture rule.

The lattice parameter for Zr^{4+} and Nb^{5+} doped ferrites, however, shows monotonic rise upto 0.0886 mole fraction for Zr^{4+} and 0.0053 mole fraction for Nb^{5+} per mole of Ni-Zn-ferrite indicating limited solid solubility. The measured density, however, shows a drastic drop followed by a monotonic rise after the solid solubility for Niobium and Zirconium shows a comparative flattening off. Both phenomena can be partially explained on the arithmatic mean density and in addition for Nb^{5+} due to change in its valency state.

The values for magnetic saturation moments for all the doped materials show a drop at lower percentages (0.0079 mole fraction for Ti^{4+}, 0.0051 mole fraction for Zr^{4+} and 0.0003 mole fraction for Nb^{5+} per mole Ni-Zn-ferrite) followed by gradual rise, levelling and falling off.

In none of these cases the sudden drop could be explained although a similar change has been observed in all cases.

Values of saturation moment theoretically determined assuming B site occupancy for Ti^{4+} show one broad evidence of our models with exception that calculated values do not explain the sudden drop followed by rise. Beyond solid solution range for Zr^{4+} and Nb^{5+}, magnetic saturation moment more or less follows a mixture rule. Titanium also shows a decrease in solubility at higher percentages and partly follows mixture rule.

TABLE - 1 : Ionic radii and atomic weights of component elements

Elements	Atomic Weight	Normal Valency State	Ionic Radius (Å)
Nickel (Ni)	58.71	2+	0.69
Zinc (Zn)	65.38	2+	0.75
Iron (Fe)	55.85	2+	0.77
		3+	0.65
Titanium (Ti)	47.90	4+	0.61
Zirconium (Zr)	91.22	4+	0.72
Niobium (Nb)	92.91	5+	0.64

TABLE - 2 : Batch compositions

Type of Batch	Component	Composition (parts)	Molecular Weight	Composition (Weight %)	Compound	Grade	Yield of Oxide per gram (Considering wt. change)	Percent Weight of Compound
Actual material	NiO	25.00	74.71	15.71	$NiCO_3$, $2Ni(OH)_2$, $4H_2O$	A.R.	1.6799	23.84
	ZnO	25.00	81.38	17.11	ZnO	A.R.	1.0000	15.45
	Fe_2O_3	50.00	159.70	77.18	Fe_2O_3	A.R.	1.0011	60.70
Packing material	NiO	25.25	74.71	15.92	Ni_2O_3	L.R.	1.064	16.77
	ZnO	25.25	81.38	17.34	ZnO	L.R.	1.000	17.17
	Fe_2O_3	49.50	159.70	66.73	Fe_2O_3	L.R.	1.000	66.06

TABLE - 3 : Dopant content of Titania doped ferrite

Solution	Normal dopant per 100gm ferrite* (percent wt.)	Volume of solution required (ml.)	Solution added (ml.)	Actual dopant used		Sample number
				gm TiO_2 per 100 gm. of ferrite	mole Ti per mole of ferrite	
a	0.2	0.754	0.900	0.2646	0.0079	1T
	0.8	3.014	3.350	0.8907	0.0240	2T
b	3.2	6.059	6.700	3.9209	0.1169	3T
	12.8	24.235	26.825	14.1681	0.4217	4T

Strength of dopant solutions:

a) 0.005 gm. Ti-metal in 1 ml.dil.H_2SO_4 (18N)

b) 0.01 gm. Ti-metal in 1 ml.dil.H_2SO_4 (18N)

*$Ni_{0.5}\ Zn_{0.5}\ Fe_2O_4$

TABLE - 4 : X-ray diffraction lines of ferrite compared with ASTM X-ray data (Reference No.8-234)

ASTM X-ray data for Ni-Zn-ferrite			Ferrite (Base material)	
d Å	I/I_1	hkl	d Å	I/I_1
4.85	14	111	-	-
2.966	45	220	2.961	32
2.699	4	211	-	-
2.533	100	311	2.525	100
2.423	6	222	2.423	4
2.100	25	400	2.094	14
1.715	10	422	1.712	8
1.617	25	511,333	1.612	27
1.485	35	440	1.483	34
1.417	2B	531	-	-
1.327	2	620	-	-
1.280	8	533	1.281	7
1.212	2	444	-	-
1.174	<1 B	551,711	-	-
1.122	4	642	-	-
1.093	12	553,731	1.094	11
1.049	6	800	-	-
-	-	844	0.858	10

X-ray unit - XRD 5 (G.E.C.)

Target - $Cu_{K\alpha}$

X-ray slit width - 3°

Receiving slit width - 0.2°

Scan speed - 2°min.

Chart speed - 1 inch/min.

TABLE - 5 : Point count intensities of X-ray diffraction readings for Titania doped Ni-Zn-ferrite

2θ	30.18°		35.55°		62.65°		74.00°		89.60°	
	Angle (degrees)	Counts (number)	Angle (degrees)	Counts (Number)	Angle (degrees)	Counts (number)	Angle (degrees)	Counts (number)	Angle (degrees)	Counts (number)
					Ni-Zn-ferrite (B)					
	30.056	25374	35.408	76453	62.502	20979	73.932	4670	89.572	4801
	30.058	25616	35.410	76616	62.504	21196	73.934	4684	89.574	4860
	30.060	25958	35.412	76953	62.506	21339	73.936	4738	89.576	4906
	30.062	26634	35.414	77235	62.508	21521	73.938	4792	89.578	4952
	30.064	27159	35.416	77544	62.510	22343	73.940	4817	89.580	4977
	30.066	26377	35.418	77100	62.512	21606	73.942	4809	89.582	4956
	30.068	25643	35.420	76831	62.514	21236	73.944	4768	89.584	4912
	30.070	25372	35.422	76619	62.516	20999	73.946	4733	89.586	4870
	30.072	25073	35.424	76174	62.518	20808	73.948	4702	89.588	4822
					1T					
	30.050	26121	35.400	75112	62.492	19531	73.930	4771	89.568	4718
	30.052	26411	35.402	75350	62.494	19711	73.932	4790	89.570	4758
	30.054	26702	35.404	75572	62.496	19952	73.934	4799	89.572	4791
	30.056	26935	35.406	75651	62.498	19999	73.936	4812	89.574	4840
	30.058	27107	35.408	75701	62.500	20105	73.938	4816	89.576	4872
	30.060	26899	35.410	75635	62.502	20097	73.940	4808	89.578	4832
	30.062	26671	35.412	75560	62.504	19985	73.942	4801	89.580	4799
	30.064	26401	35.414	75343	62.506	19800	73.944	4789	89.582	4764
	30.066	26087	35.416	75091	62.508	19652	73.946	4765	89.584	4715

Continued...

TABLE - 5 (continued)

2T

30.038	27640	35.386	72008	62.478	19185	73.922	3456	89.568	4121
30.040	27838	35.388	72507	62.480	19275	73.924	3483	89.570	4134
30.042	28074	35.390	72970	62.482	19355	73.926	3570	89.572	4182
30.044	28162	35.392	73010	62.484	19382	73.928	3645	89.574	4188
30.046	28320	35.394	73635	62.486	19579	73.930	3684	89.576	4253
30.048	28198	35.396	73203	62.488	19459	73.932	3637	89.578	4193
30.050	27644	35.398	73134	62.490	19404	73.934	3605	89.580	4150
30.052	27581	35.400	72516	62.492	19141	73.936	3592	89.582	4132
30.054	27482	35.402	72205	62.494	19052	73.938	3556	89.584	4114

3T

30.018	23254	35.368	88316	62.448	17033	73.870	3709	89.502	4642
30.020	23478	35.370	88426	62.450	17151	73.872	3734	89.504	4790
30.022	23667	35.372	88547	62.452	17378	73.874	3785	89.506	4833
30.024	23995	35.374	89246	62.454	17505	73.876	3878	89.508	4882
30.026	24136	35.376	90032	62.456	17697	73.878	3950	89.510	4925
30.028	23929	35.378	89340	62.458	17495	73.880	3892	89.512	4837
30.030	23632	35.380	88676	62.460	17375	73.882	3834	89.514	4791
30.032	23441	35.382	88227	62.462	17172	73.884	3785	89.516	4712
30.034	23215	35.384	87989	62.464	17056	73.886	3762	89.518	4655

4T

29.996	17158	35.342	48554	62.406	12318	73.836	2505	89.446	2975
29.998	17221	35.344	48761	62.408	12349	73.838	2546	89.448	2989
30.000	17286	35.346	49084	62.410	12385	73.840	2573	89.450	3011
30.002	17317	35.348	49360	62.412	12447	73.842	2602	89.452	3026
30.004	17439	35.350	49518	62.414	12522	73.844	2635	89.454	3050
30.006	17443	35.352	49545	62.416	12435	73.846	2611	89.456	3054
30.008	17186	35.354	49403	62.418	12350	73.848	2588	89.458	3031
30.010	17151	35.356	49315	62.420	12321	73.850	2555	89.460	3015
30.012	17105	35.358	49203	62.422	12308	73.852	2541	89.462	2091

Note:- All counts were taken for 60 seconds.

TABLE - 6 : Estimation of lattice parameter of Titania doped ferrite using Nelson-Riley function

Sample Number	Gram TiO_2 per 100 gm ferrite	Mole Dopant per mole of ferrite	2θ (degree)	θ (degree)	d (Å)	hkl	Lattice Parameters for Different d-values (Å)	Nelson-Riley Function f(θ)	Extrapolated Value of Lattice Parameter (Å)
B	0	0	30.064	15.032	2.969828	220	8.399412	3.5744	
			35.416	17.708	2.532334	311	8.398812	2.9598	
			62.510	31.255	1.484539	440	8.397822	1.3741	8.39745
			73.941	36.970	1.280753	533	8.398462	1.0253	
			89.580	44.790	1.093312	553	8.397893	0.6792	
1T	0.2646	0.0079	30.058	15.029	2.970407	220	8.401752	3.5692	
			35.408	17.704	2.532887	311	8.400637	2.9601	
			62.501	31.250	1.484731	440	8.398908	1.3744	8.39694
			73.938	36.969	1.280799	533	8.398755	1.0253	
			89.576	44.788	1.093351	553	8.397884	0.6796	
2T	0.8907	0.0240	30.046	15.023	2.971566	220	8.404858	3.5781	
			35.394	17.697	2.533857	311	8.403854	2.9620	
			62.486	31.243	1.485052	440	8.400721	1.3749	8.39510
			73.930	36.965	1.280917	533	8.399534	1.0309	
			89.576	44.788	1.093351	553	8.397881	0.6796	
3T	3.9209	0.1169	30.026	15.013	2.974465	220	8.413057	3.5807	
			35.376	17.688	2.535105	311	8.407992	2.9638	
			62.456	31.228	1.485693	440	8.404349	1.3760	8.40330
			73.878	36.939	1.281690	533	8.404603	1.0273	
			89.510	44.755	1.093986	553	8.403066	0.6809	
4T	14.1681	0.4217	30.005	15.002	2.975523	220	8.416050	3.5842	
			35.352	17.676	2.536771	211	8.413587	2.9662	
			62.414	31.207	1.486592	440	8.409434	1.3774	8.40459
			73.844	36.922	1.282196	533	8.407723	1.0278	
			89.455	44.727	1.094370	553	8.406026	0.6818	

Continued...

TABLE - 6 : Estimation of lattice parameter of Zirconia doped ferrite using Nelson-Riley Function (Continued)

Sample Number	Gram ZrO_2 per 100 gm ferrite	Mole Dopant per mole of ferrite	2θ (degree)	θ (degree)	d (Å)	hkl	Lattice Parameters for Different d-values (Å)	Nelson-Riley Function f(θ)	Extrapolated value of Lattic Parameter (Å)
B	0	0	35.27	17.635	2.542482	311	8.432457	3.9893	8.39360
			62.40	31.200	1.486892	440	8.411312	1.3779	
			89.51	44.755	1.093986	553	8.403066	0.6707	
			128.03	64.015	0.856891	844	8.395783	0.1929	
1Z	0.2216	0.0051	35.24	17.620	2.544577	311	8.439407	3.9767	8.39525
			62.37	31.185	1.487535	440	8.414769	1.3790	
			89.47	44.735	1.094371	553	8.406023	0.6816	
			127.97	63.985	0.857091	844	8.397742	0.1931	
2Z	0.8864	0.0231	35.24	17.620	2.544577	311	8.439407	3.9767	8.39800
			62.35	31.175	1.487964	440	8.417093	1.3797	
			89.45	44.725	1.094564	553	8.407505	0.6820	
			127.89	63.945	0.857383	844	8.400593	0.1938	
3Z	3.4031	0.0886	35.24	17.620	2.544577	311	8.439407	3.9767	8.39900
			62.33	31.165	1.488393	440	8.419624	1.3804	
			89.43	44.765	1.094757	553	8.408988	0.6805	
			127.85	63.925	0.857530	844	8.402044	0.1941	
4Z	14.1903	0.3696	35.23	17.630	2.542577	311	8.441728	3.9753	8.39900
			62.34	31.170	1.488179	440	8.418412	1.3801	
			89.45	44.725	1.094564	553	8.407505	0.6820	
			127.85	63.925	0.857530	844	8.402044	0.1941	

Continued...

TABLE - 6 : Estimation of lattice parameter of Nb_2O_5 doped ferrite using Nelson-Riley function (Continued)

Sample Number	Gram Nb_2O_5 per 100 gm ferrite	Mole Dopant, Nb per mole of ferrite	2θ (degree)	θ (degree)	d (Å)	hkl	Lattice Parameters for Different d-values (Å)	Nelson-Riley Function f(θ)	Extrapolated Value of Lattice Parameter (Å)
1N	0.2216	0.0003	35.26	17.630	2.543180	311	8.434774	3.9753	8.39515
			62.37	31.185	1.487535	440	8.414768	1.3790	
			89.49	44.745	1.094179	553	8.404545	0.6812	
			127.96	63.980	0.857128	844	8.398101	1.1932	
2N	0.8864	0.0012	35.25	17.625	2.543879	311	8.437091	3.9763	8.39800
			62.34	31.170	1.488179	440	8.418410	1.3801	
			89.47	44.735	1.094371	553	8.406026	0.6816	
			127.89	63.945	0.805738	844	8.400608	0.1930	
3N	3.9888	0.0053	35.25	17.625	2.543879	311	8.437091	3.9763	8.39800
			62.34	31.170	1.488179	440	8.418410	1.3801	
			89.45	44.750	1.094564	553	8.407508	0.6810	
			127.88	63.940	0.857420	844	8.400967	0.1989	
4N	14.1824	0.0188	35.25	17.625	2.543879	311	8.437091	3.9763	8.39815
			62.34	31.170	1.488179	440	8.418410	1.3801	
			89.45	44.725	1.094564	553	8.407508	0.6820	
			127.87	63.935	0.857457	844	8.401325	0.1939	

TABLE - 7 : Pycnometic density values of ferrite compositions

Sample	Measured density in gms/ml.	Standard deviation
Ni-Zn-ferrite(B)	5.2576	0.0455
1T	5.2909	0.0553
2T	5.3372	0.0608
3T	5.1450	0.0153
4T	5.0270	0.0451
TiO_2	4.0297	0.0296
1Z	5.2064	0.0513
2Z	5.1377	0.0346
3Z	5.2636	0.0170
4Z	5.2216	0.0409
ZrO_2	5.6911	0.0503
1N	5.2284	0.0351
2N	5.0770	0.0231
3N	5.1103	0.0574
4N	5.3372	0.0608
Nb_2O_5	4.6728	0.0021

TABLE - 8 : Table showing the variation of magnetic moment of Ni-Zn-ferrite (base composition) with applied magnetic field at room temperature*

Applied field (K.Oe)	Magnetic Moment (emu)x10	(emu/gm.)
0.5	0.362	32.04
1.0	0.595	52.65
1.5	0.704	62.30
2.0	0.752	66.55
2.5	0.774	68.49
3.0	0.788	69.73
3.5	0.796	70.44
4.0	0.802	70.97
4.5	0.806	71.32
5.0	0.809	71.59
5.5	0.812	71.85
6.0	0.814	72.04
6.5	0.816	72.21

*Room Temperature = 25.7°C
Mass of the sample = 0.1130 gm.

TABLE - 9 : Saturation magnetic moment of Ni-Zn-ferrite compositions with different dopants at room temperature

Sample	Mass* (gms.)	Residual Magnetisation (emu per sample)	Residual Magnetisation (emu/gm)	Magnetic moments (emu per sample)x10	Magnetic moments σ_s (emu/gm.)	Mean σ_s (emu/gm.)	$4\pi M_s^+$ (Gauss)
B1	0.1130	0.241	2.132	0.816	72.21	71.44	4719.9
B2	0.0965	0.233	2.414	0.682	70.67		
1T1	0.1225	0.273	2.730	0.804	65.63	67.68	4499.8
1T2	0.1037	0.256	2.468	0.723	69.72		
2T1	0.1292	0.317	2.453	0.882	68.27	68.68	4508.0
2T2	0.1019	0.267	2.620	0.704	69.09		
3T1	0.1292	0.317	2.453	0.871	67.41	68.20	4409.4
3T2	0.1238	0.314	2.536	0.854	68.98		
4T1	0.0962	0.234	2.432	0.447	46.47	47.23	2983.5
4T2	0.0952	0.233	2.447	0.457	48.00		
1Z1	0.1347	0.343	2.546	0.786	58.35	58.73	3842.4
1Z2	0.1020	0.212	2.078	0.603	59.11		
2Z1	0.1259	0.247	1.962	0.734	58.30	60.42	3900.8
2Z2	0.0849	0.214	2.526	0.531	62.54		
3Z1	0.1195	0.245	2.050	0.723	60.50	60.49	4001.7
3Z2	0.1136	0.242	2.130	0.687	60.47		
4Z1	0.1388	0.275	1.981	0.747	53.82	53.88	3535.4
4Z2	0.1179	0.247	2.095	0.636	53.94		
1N1	0.1269	0.284	2.238	0.782	61.62	61.97	4071.5
1N2	0.0889	0.219	2.463	0.554	62.31		

Continued....

TABLE - 9 (continued)

Sample	Mass* (gms.)	Residual Magnetisation (emu per sample)	Residual Magnetisation (emu/gm)	Magnetic moments (emu per sample)x10	Magnetic moments σ_s (emu/cm.)	Mean σ_s (emu/cm.)	$4\pi M_s^+$ (Gauss)
2N1	0.1183	0.253	2.139	0.754	63.74	63.33	4040.4
2N2	0.1241	0.272	2.192	0.781	62.93		
3N1	0.1315	0.271	2.061	0.792	60.22	63.24	4061.1
3N2	0.0993	0.257	2.588	0.658	66.26		
4N1	0.1211	0.262	2.163	0.715	59.04	59.46	3987.8
4N2	0.1249	0.280	2.242	0.748	59.88		

Applied magnetic field = 6,5 K.Oes.

* Mass of P.V.A. binder excluded.

+ M_s = Saturation magnetisation (Gauss cm^3/gm)x density (gms/ml.)

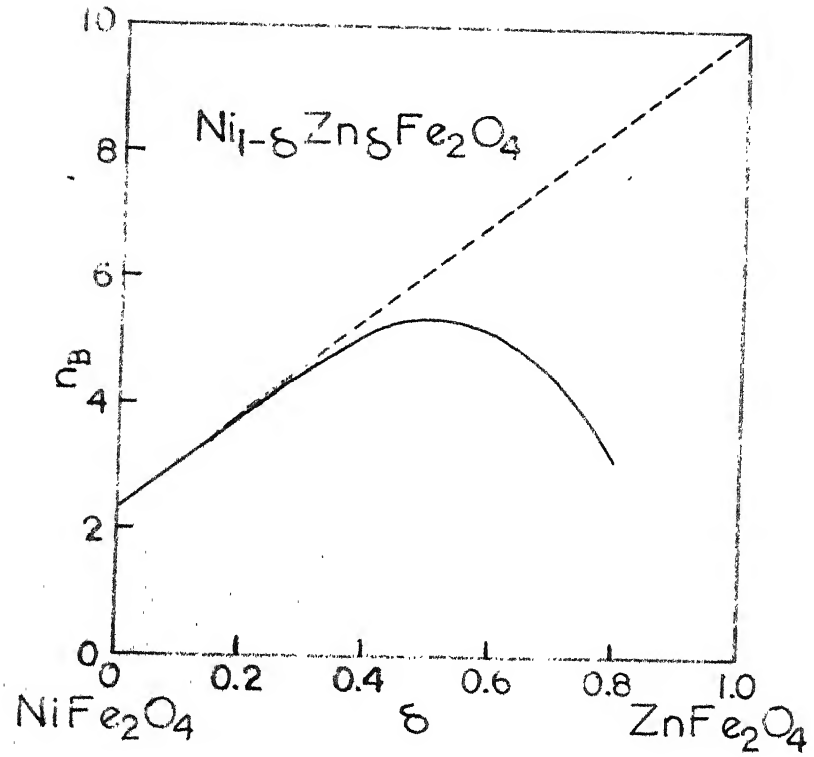

Fig. 1(a) Saturation moment in Bohr magneton at 0°K for Ni-Zn-ferrites

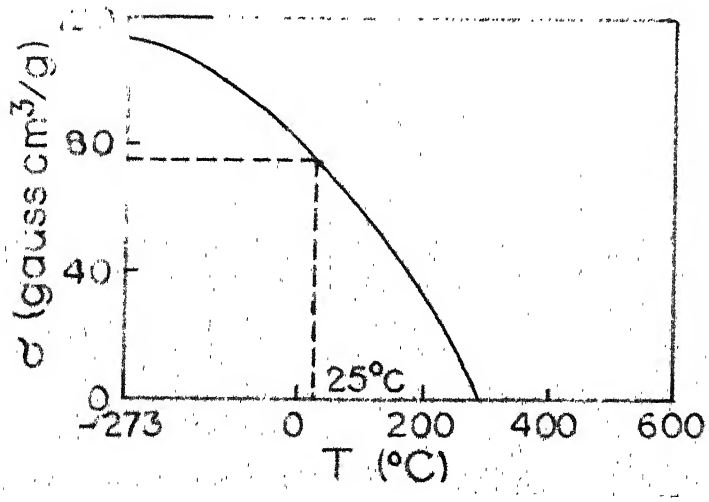

Fig. 1(b) Saturation magnetisation per gm., σ, as a function of temperature for $Ni_{0.5}Zn_{0.5}Fe_2O_4$

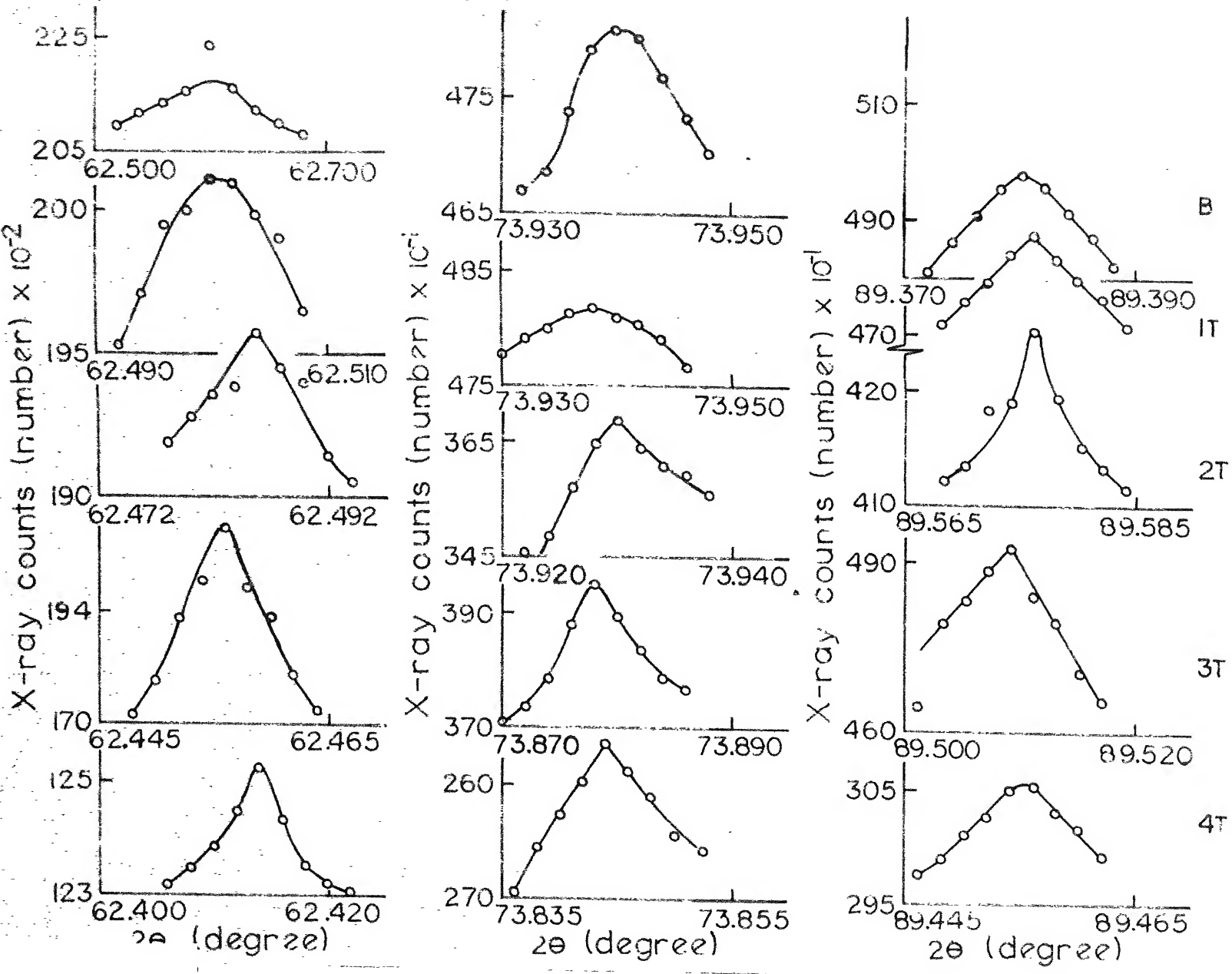

Fig. 2 Plot of X-ray counts versus 2θ for d-value determination by point count method

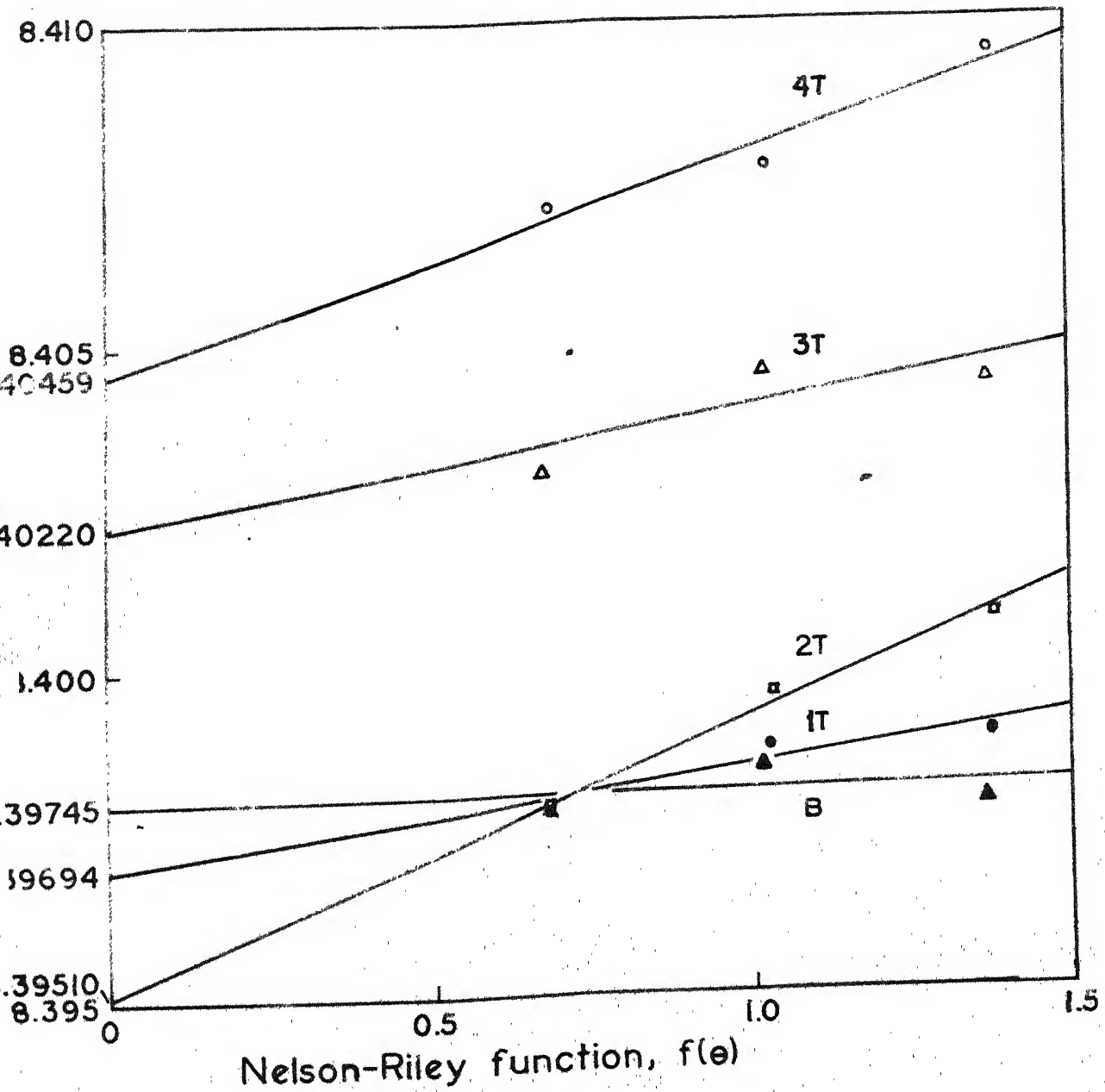

Fig. 3 Plot of lattice parameter, a, versus Nelson-Riley function, f(θ), for Ni-Zn-ferrite compositions doped with Titanium

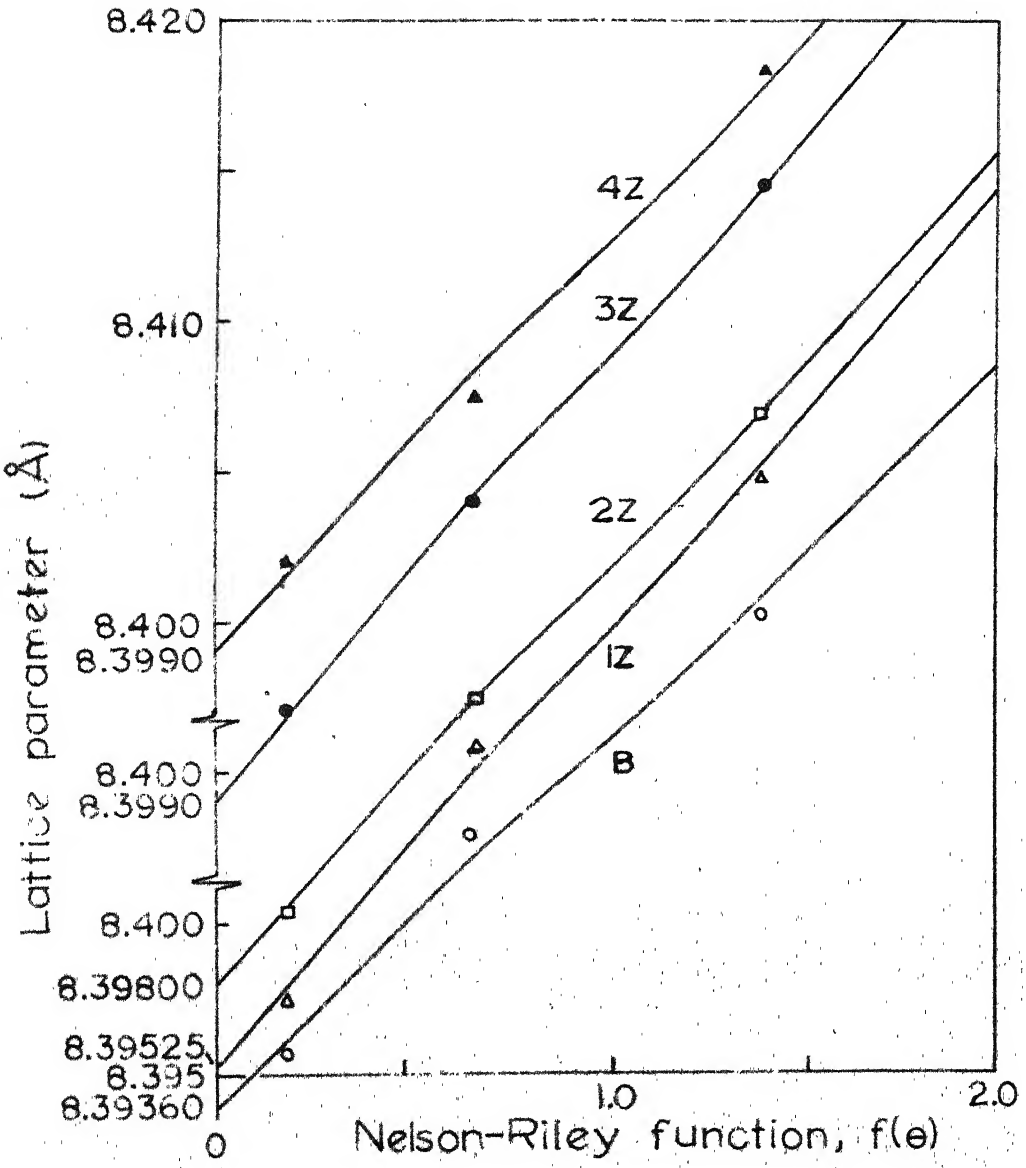

Fig. 4 Plot of lattice parameter, a, versus Nelson-Riley function, f(θ), for Ni-Zn-ferrite compositions doped with Zirconium

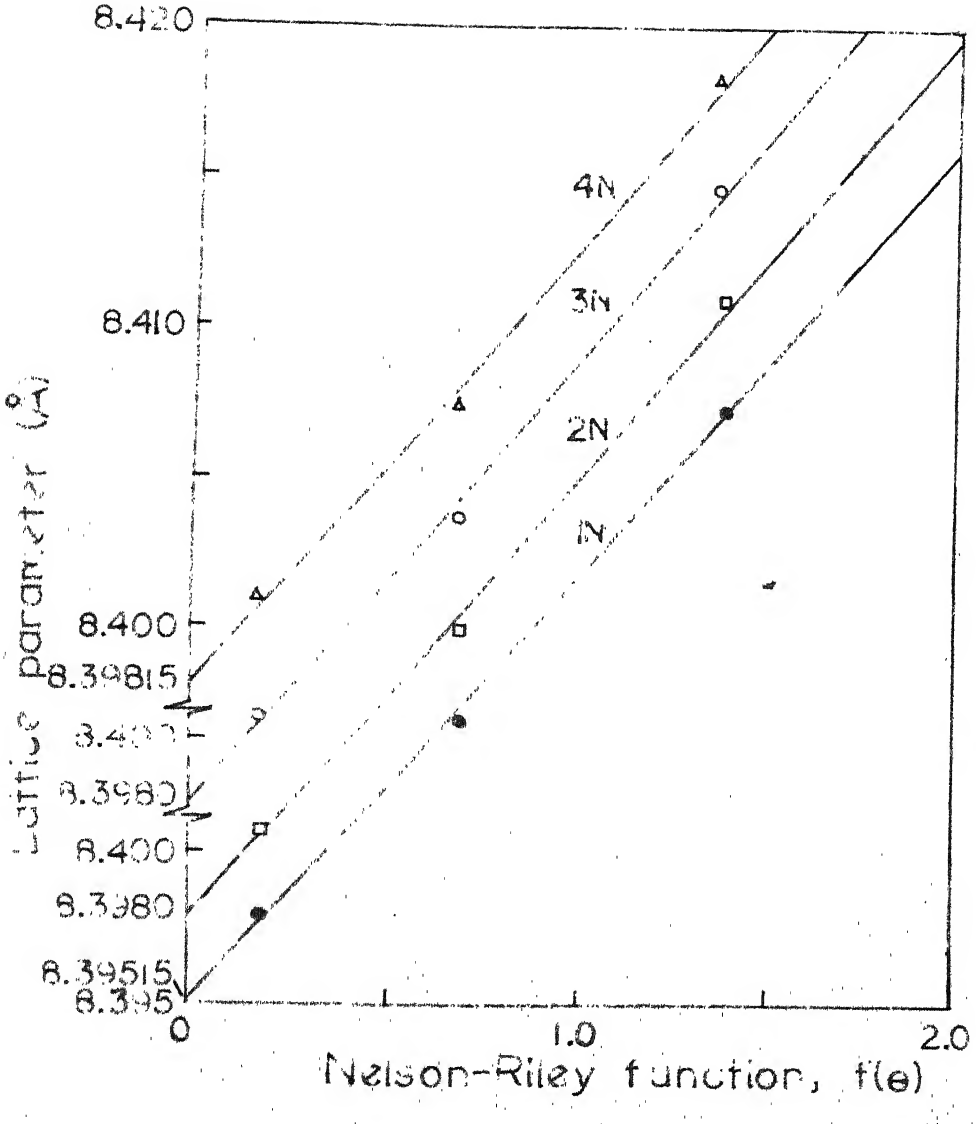

Fig. 5 Plot of lattice parameter, a, versus Nelson-Riley function, f(θ), for Ni-Zn-ferrite compositions doped with Niobium

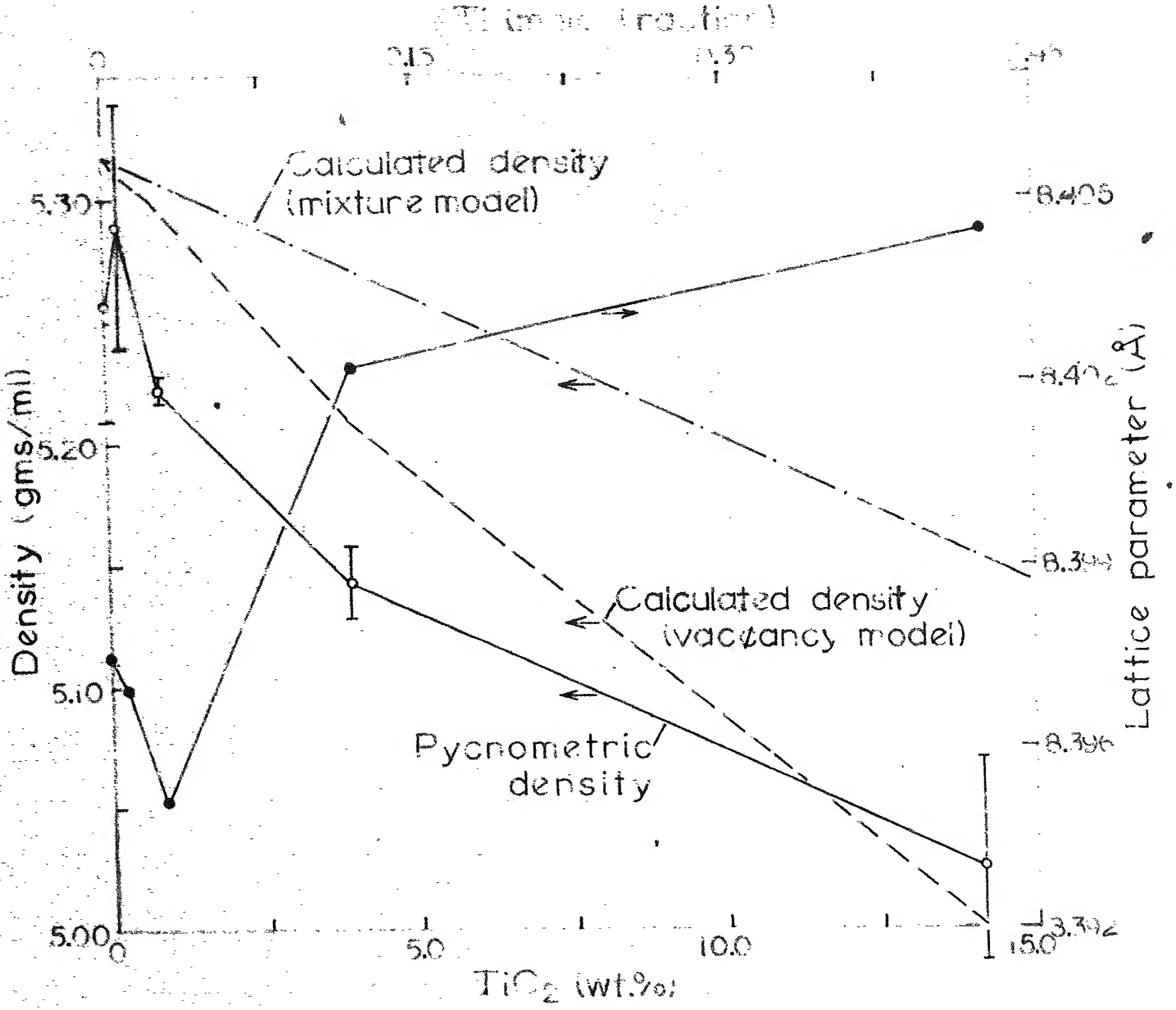

Fig. 6 Plots of density and lattice parameter for Ti-doped Ni-Zn-ferrite

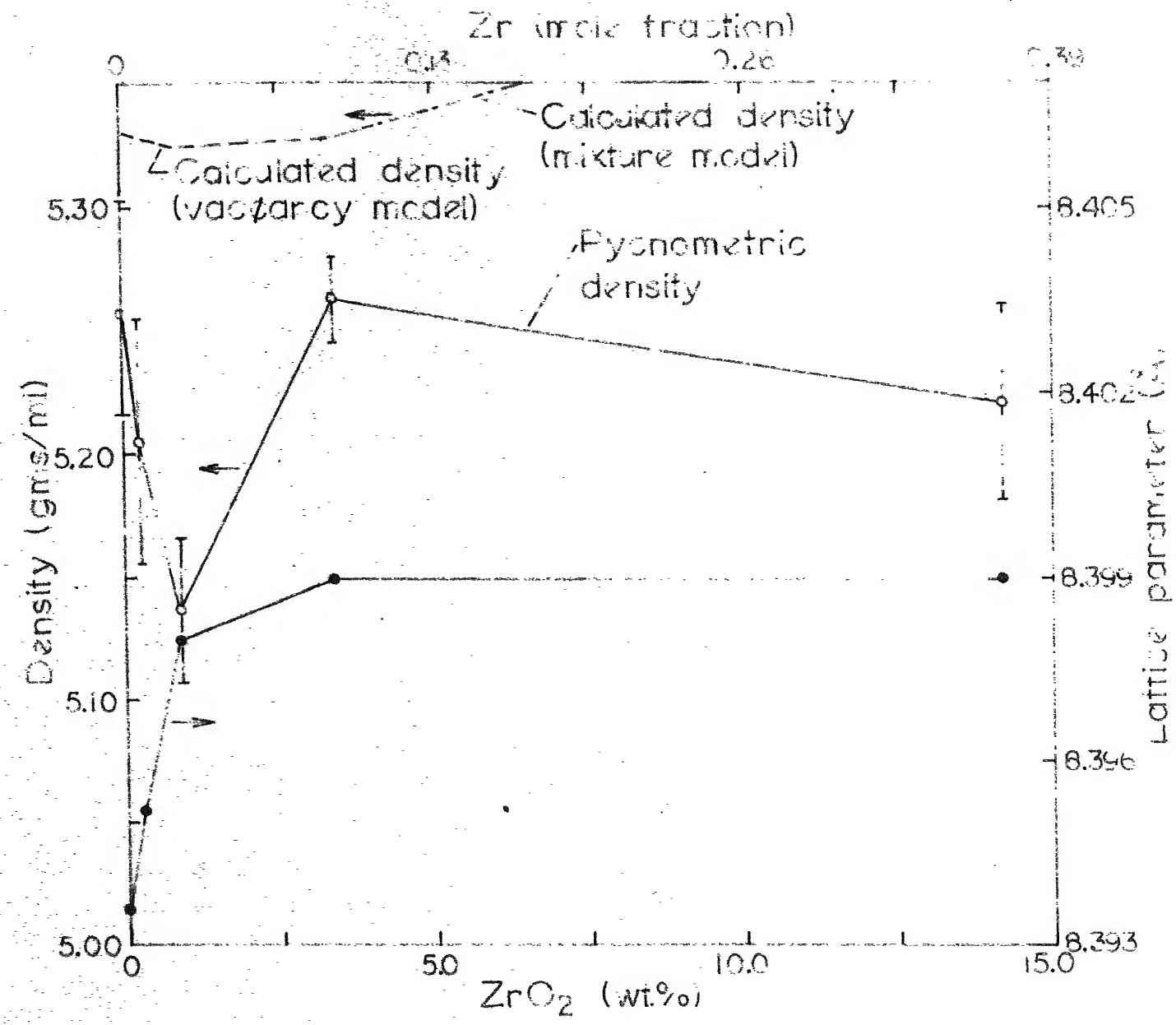

Fig. 7 Plots of density and lattice parameter for

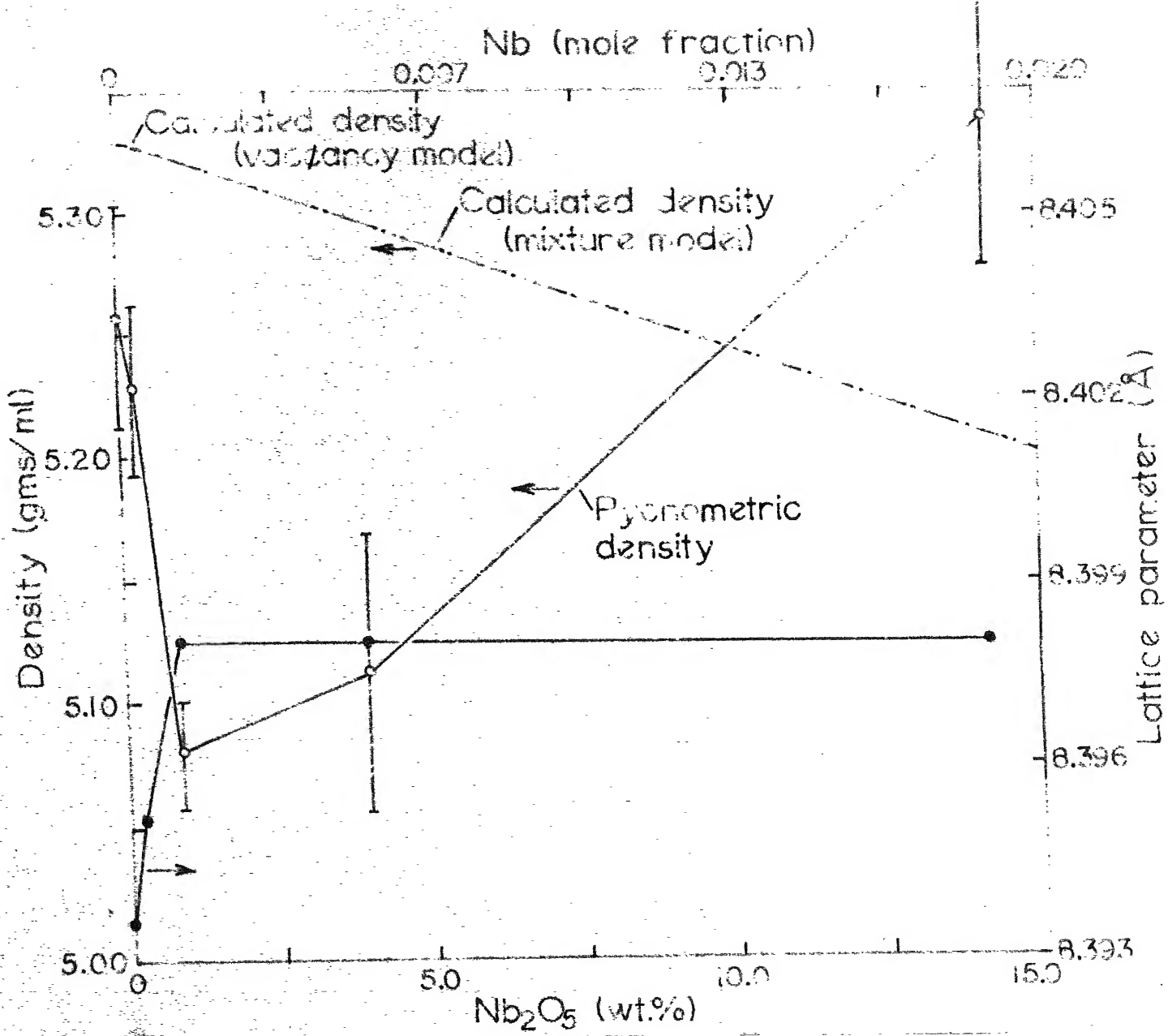

Fig. 8 Plots of density and lattice parameter for

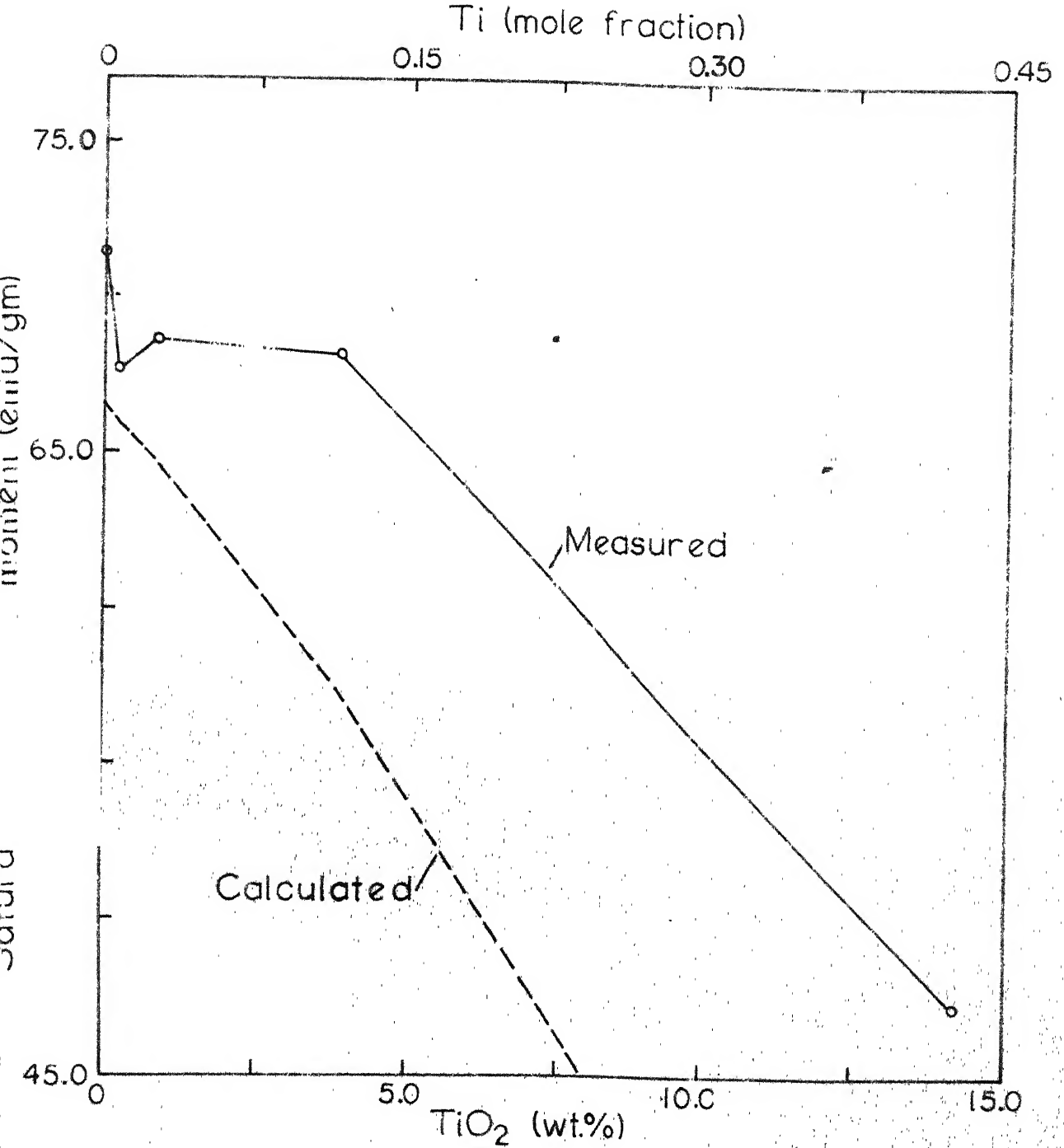

Fig. 9 Plots of saturation magnetic moment versus dopant content for $Ni_{0.5}Zn_{0.5}Fe_2O_4$ doped with Titanium

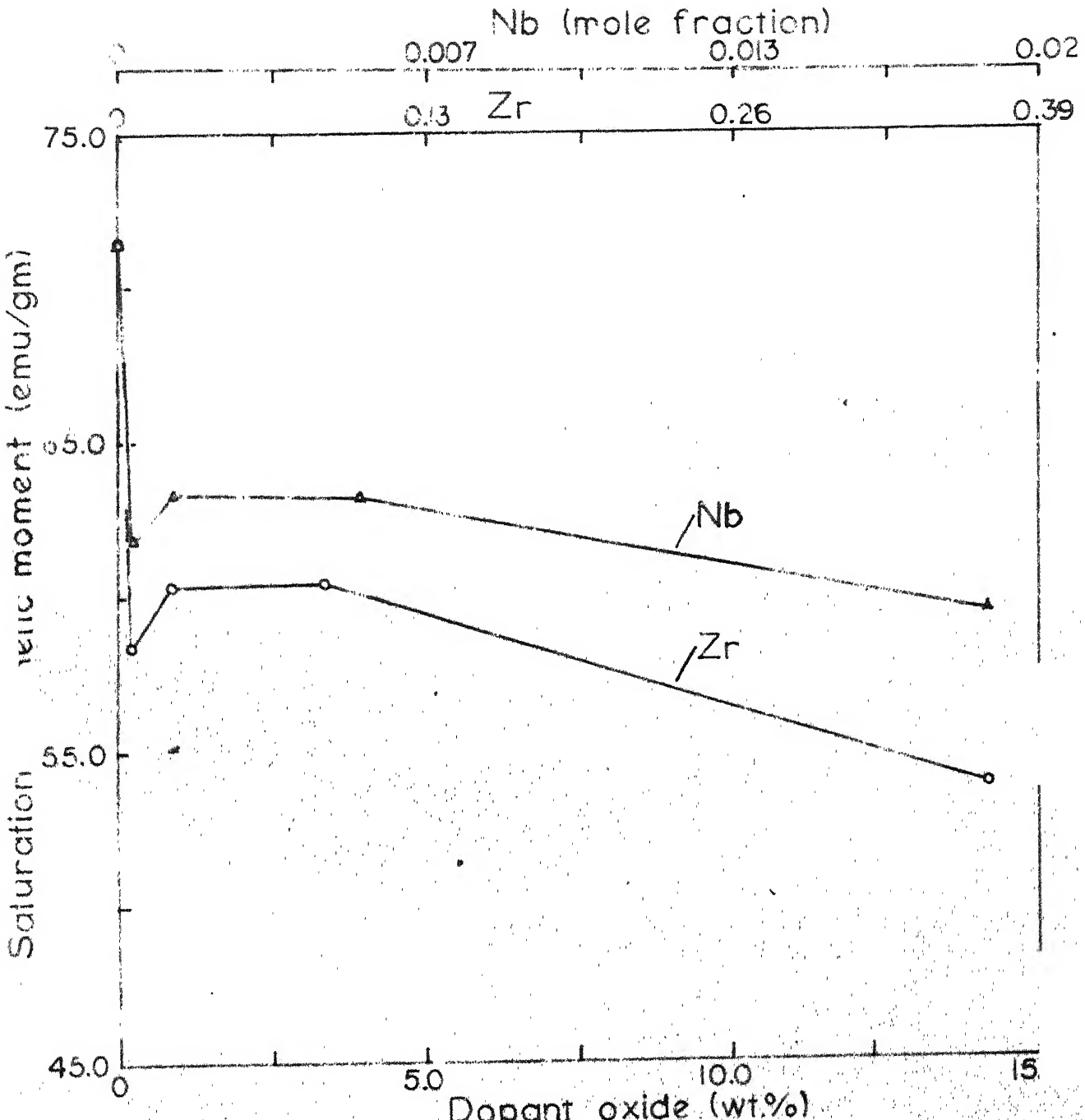

Fig. 10 Plots of saturation magnetic moment versus dopant content for $Ni_{0.5}Zn_{0.5}Fe_2O_4$ doped with Zirconium and Niobium

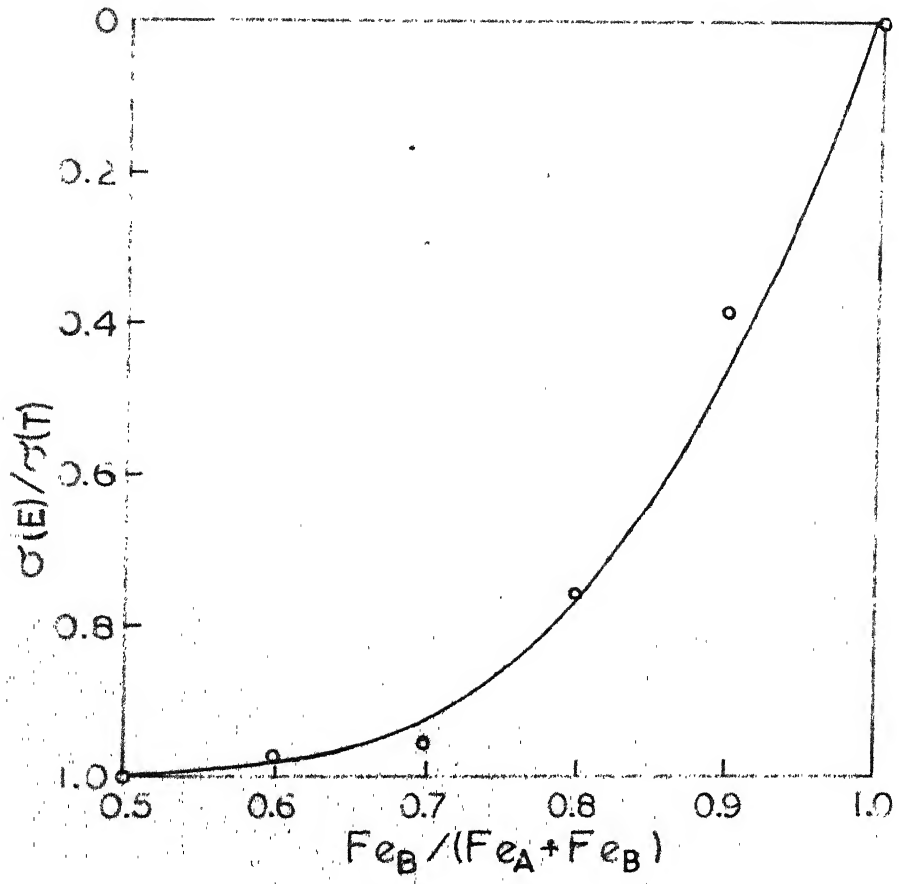

Fig. 11 Plot of the ratio of the experimental magnetic moment to the theoretical value $\sigma(E)/\sigma(T)$ for Ni-Zn-ferrite versus $Fe_B/(Fe_A + Fe_B)$, the numbers of Fe in B sites to the total Fe

REFERENCES

1. B.D. Cullity, "Introduction to magnetic materials" - Addition-Wesley Publishing Co. New York (1972), p. 551.

2. F.N. Bradley, "Materials for magnetic functions" - Hayden Book Co. Inc. New York, (1971), p. 61.

3. A.B. Groenou, P.F. Bongers and A.L. Stuyts, "Magnetism, microstructure and crystal chemistry of spinel ferrites" - Mat. Sci. Eng., 3, (1968), p. 322.

4. ibid., p. 323.

5. W.D. Kingery, "Introduction to Ceramics" - John Wiley & Sons, New York, (1963), p. 753.

6. C. O'Hara et.al.,"The influence of sintering conditions on the magnetic properties of Mn-Zn-ferrite - Proc. Brit. Cer. Soc., 10, (1968), p. 245-262.

7. P.I. Slick and H. Blasscheb, "Thermogravimetric study of the solid gas interaction of a Mn-Zn-ferrite and the effect on its magnetic properties" - I.E.E.E. Trans. (Magnetics), MAG-2, (1966), p. 603-607.

8. A. Sen, "Effect of Titaina addition on magnetic spectrum and saturation magnetisation of $Ni_{0.3}Zn_{0.7}Fe_2O_4$" - M. Tech. Thesis, I.I.T. Kanpur, (1978), p. 8.

9. R.S. Tebble and D.J. Craik, "Magnetic materials" - Wiley Interscience,London, (1969), p. 562.

10. E.W. Gorter, "Saturation magnetication and crystal chemistry of ferrimagnetic oxides", Philips Res. Rep. 9, (1954), p. 403-443.

11. Stintjes et.al. "Permeability and conductivity of Ti-substituted Mn-Zn-ferrite"- Philips Res. Rep. 25(2), (1970), p. 95.

12. A. Sen, "Effect of Titania addition on magnetic spectrum and saturation magnetisation of $Ni_{0.3}Zn_{0.7}Fe_2O_4$" - M. Tech. Thesis, I.I.T. Kanpur, (1978), p. 9.

13. J.E. Knowles, "Magnetic after effects in ferrites substituted with Ti or Sn" - Philip Res. Rep. 29, (1974), p. 93.

14. G. Blasse, "Crystal chemistry and some magnetic properties of mixed metal oxides with spinel structure" - Philips. Res. Rep., 19S3, (1964).

15. ibid., p. 103-104.

16. J. Smit and H.P. J. Wijn ,"Ferrites" - Philips Technical Library Eindhoven (Holland), (1958), p. 145.

17. Kedesky and Katz, Ceramic Age 62 (1953), p. 29-34.

18. A.S.T.M. Powder diffraction file No. 8-234.

19. V.R.K. Murthy, et.al., "X-ray diffraction and saturation magnetisation studies of some Ni-Zn-ferrites" - Rev. Roun. Phys. 22(8), (1977), p. 821-6 (Eng.); Chem. Abs. 88 (1978), p. 68403f.

20. S.K. Gupta, "Effect of processing conditions and microstructure on the magnetic spectrum of Ni-Zn-Ferrite" - M. Tech. Thesis, I.I.T., (1976), p. 15a.

21. Ed. R.C. Weast, "Hand book of Physics and Chemistry" - CRC Press Inc., Cleveland (Ohio) (1977), p. B136.

22. E.W. Gorter, "Saturation magnetisation and crystal chemistry of ferrimagnetic oxides", Philips Res. Rep. 9, (1954), p. 404.

23. K.P. Gupta, et.al., "Experiments in X-ray diffraction" I.I.T. Kanpur, p. 69.

24. K.P. Gupta and S.P. Bhat, "X-ray data book for analysis of Laue and powder diffraction patterns" - Department of Met. Engg., I.I.T. Kanpur (1974), p. 174.

APPENDIX[23,24]

The position of diffraction lines in a diffraction pattern gives the diffraction angle 'θ' using which the interplaner spacing 'd' can be determined using Bragg's equation,

$$\lambda = 2d \sin\theta$$

On indexing the diffraction lines, the 'd' spacings, the (hkl) indices and the relation $a = d(h^2+k^2+l^2)^{1/2}$, lattice parameter (a) can be determined. This simple procedure is applicable to only those structures which have orthogonal axes system or which can be converted to a structure with orthogonal axes (viz. hexagonal, trigonal or rhombohedral).

The error in diffraction angle is due to

i) systematic errors, which is dueto specific geometrical and physical reasons and is always in one direction, and

ii) random errors, due to error in locating the exact position of a diffraction line which always has a certain width and gives both negative and positive deviations from the true diffraction angle. The lattice parameter is found to decrease with decreasing diffraction angle.

On differentiating Bragg's law, we get,

$$\frac{\Delta d}{d} = - \cot\theta . \Delta\theta$$

which indicates that $\frac{\Delta d}{d} \rightarrow 0$ as, $\theta \rightarrow 90°$. Thus precise value of lattice parameter can be obtained by extrapolating the lattice parameter to $\theta = 90°$ using a suitable extrapolation function.

It is necessary especially for highly symmetric crystals like the cubic crystals, to use low angle reflections for extrapolation of lattice parameters. The fractional error in this case is given by

$\frac{\Delta a}{a_o} = K \left(\frac{\cos^2\theta}{\sin^2\theta} + \frac{\cos^2\theta}{\theta}\right)$, where 'K' is the fractional error constant.

The extrapolation function is known as Nelson-Riley function. This extrapolation function is linear i.e. if lattice parameter for different refracted angles are plotted with the function,

$$f(\theta) = \frac{\cos^2\theta}{\sin^2\theta} + \frac{\cos^2\theta}{\theta}$$

the curve will be a straight line and the value of the lattice parameter corresponding to $f(\theta) = 0$ will be the most accurate.

The random error can be minimised by careful measurement of diffraction line positions and can be done by point count method. The scattering in the plotted data can be minimised by the method of least squares to determine the most probable value of the lattice parameter.

ME-1981-M-DAS-EFF